

1 **Impact of fossil and non-fossil sources on the molecular compositions of water soluble humic-**
2 **like substance in PM_{2.5} at a suburb site of Yangtze River Delta, China**

3
4 Mengying Bao^{1,2,3}, Yan-Lin Zhang^{1,2,*}, Fang Cao^{1,2}, Yihang Hong^{1,2}, Yu-Chi Lin^{1,2}, Mingyuan Yu^{1,2},
5 Hongxing Jiang^{4,5}, Zhineng Cheng^{4,5}, Rongshuang Xu^{1,2}, Xiaoying Yang^{1,2}

6
7 *1 School of Applied Meteorology, Nanjing University of Information Science & Technology,*
8 *Nanjing 210044, China.*

9 *2 Atmospheric Environment Center, Joint Laboratory for International Cooperation on Climate*
10 *and Environmental Change, Ministry of Education (ILCEC), Nanjing University of Information*
11 *Science & Technology, Nanjing 210044, China.*

12 *3 Huzhou Meteorological Administration, Huzhou 313300, China*

13 *4 State Key Laboratory of Organic Geochemistry and Guangdong province Key Laboratory of*
14 *Environmental Protection and Resources Utilization, Guangzhou Institute of Geochemistry,*
15 *Chinese Academy of Sciences, Guangzhou 510640, China.*

16 *5 CAS Center for Excellence in Deep Earth Science, Guangzhou 510640, China*

17 *Correspondence: Yan-Lin Zhang (dryanlinzhang@outlook.com)*

18

19 **Abstract**

20 Atmospheric humic-like substances (HULIS) affect global radiation balance due to their
21 strong light absorption at the ultraviolet wavelength. The potential sources and molecular
22 compositions of water soluble HULIS at a suburb site of Yangtze River Delta from 2017 to 2018
23 were discussed based on the radiocarbon (¹⁴C) analysis combining the Fourier Transform Ion
24 Cyclotron Resonance Mass Spectrometry (FT-ICR MS) technique in this study. The ¹⁴C results
25 showed that the averaged non-fossil source contributions to HULIS were 39 ± 8 % and 36 ± 6 %
26 in summer and winter, respectively, indicating the significant contributions from fossil sources to
27 HULIS. The Van Krevelen diagrams obtained from the FT-ICR MS results showed that the
28 proportions of tannins-like and carbohydrates-like groups were higher in summer, suggesting
29 significant contribution of HULIS from biogenic secondary organic aerosols (SOA). The higher
30 proportions of condensed aromatic structures in winter suggested increasing anthropogenic
31 emissions. Molecular composition analysis on the CHO, CHON, CHOS, and CHONS subgroups

32 showed the relatively higher intensities of high O-containing macromolecular oligomers in CHO
33 compounds in summer, further indicating stronger biogenic SOA formation in summer. High-
34 intensity phenolic substances and flavonoids which were related to biomass burning and polycyclic
35 aromatic hydrocarbons (PAHs) derivatives indicating fossil fuel combustion emissions were found
36 in winter CHO compounds. Besides, two high-intensity CHO compounds containing condensed
37 aromatic ring structures ($C_9H_6O_7$ and $C_{10}H_5O_8$) identified in summer and winter samples were
38 similar to those from off-road engine samples, indicating that traffic emission was one of the
39 important fossil sources of HULIS at the study site. The CHON compounds were mainly composed
40 of nitro compounds or organonitrates with significantly higher intensities in winter, which was
41 associated to biomass burning emission, as well as the enhanced formation of organonitrates due
42 to high NO_x in winter. However, the high-intensity CHON molecular formulas in summer were
43 referring to N-heterocyclic aromatic compounds, which were produced from the atmospheric
44 secondary processes involving reduced N species (e.g., ammonium). The S-containing compounds
45 were mainly composed of organosulfates (OSs) derived from biogenic precursors, long-chain
46 alkane and aromatic hydrocarbon, illustrating the mixed sources of HULIS. Generally, different
47 policies need to be considered for each season due to the different season sources, i.e., biogenic
48 emission in summer and biomass burning in winter for non-fossil source, traffic emission and
49 anthropogenic SOA formation in both seasons and additional coal combustion in winter. Measures
50 to control emissions from motor vehicles and industrial processes need to be considered in summer.
51 Additional control measures on coal power plants and biomass burning should be concerned in
52 winter. These findings add to our understanding of the interaction between the sources and the
53 molecular compositions of atmospheric HULIS.

54

55 **1. Introduction**

56 Atmospheric humic-like substances (HULIS) have been observed worldwide and can be
57 produced from primary combustion of biomass, fossil fuel, as well as various secondary processes
58 such as photochemical processes of volatile organic compounds (VOCs) and heterogeneous
59 reactions of organic aerosols in the atmosphere (Kuang et al., 2015; Li et al., 2019; Ma et al., 2018;
60 Sun et al., 2021). As important component of brown carbon (BrC) aerosols, HULIS species have
61 been widely reported to have a great impact on global radiative budget, contributing to 20-40% of
62 the direct radiative forcing caused by light absorbing aerosols due to its light absorption at the

63 ultraviolet wavelength (Chung et al., 2012; Zhang et al., 2017; Zhang et al., 2020a; Wang et al.,
64 2018c). HULIS are a highly complex mixture of polar organic compounds composed of aromatic
65 and hydrophobic aliphatic structures containing carboxyl, carbonyl, and hydroxyl function groups
66 (Zheng et al., 2013; Graber and Rudich, 2006; Zhang et al., 2022b; Zhang et al., 2022c). During
67 the atmospheric secondary oxidation processes, the substitutions of hydrophilic functional groups
68 increased aerosol hygroscopicity (Huo et al., 2021; Jiang et al., 2020). Polycarboxylic acids in
69 HULIS are surface-active and play an important role in the cloud condensation nuclei (CCN)
70 activity (Tsui and McNeill, 2018). N-base compounds can promote the generation of atmospheric
71 reactive oxygen species (ROS) which have a great impact on human health (Wang et al., 2017c;
72 De Haan et al., 2018; Song et al., 2022). Identifying the molecular compositions of HULIS is a
73 challenge due to complex mixtures contained in HULIS and can help to a better understanding of
74 the processes involving organic compounds in atmosphere (Noziere et al., 2015; Laskin et al.,
75 2018).

76 The Fourier-Transform Ion Cyclotron Resonance Mass Spectrometry (FT-ICR MS) coupled
77 with electrospray ionization (ESI) ion source have been widely used in identifying the chemical
78 structure of HULIS, providing high mass accuracy and can determine molecular formulas from
79 mixed compounds (Chen et al., 2016; Wang et al., 2019b; Lin et al., 2012a; Jiang et al., 2020).
80 Typical molecular formulas composed of C, H, and O atoms in HULIS were observed being
81 abundant in carboxylic acids, lignin-derived products, and polycyclic aromatic hydrocarbons
82 (PAHs) or their derivatives (Lin et al., 2012a; Sun et al., 2021; Jiang et al., 2020; Huo et al., 2021;
83 Song et al., 2018). In addition, the HULIS formation of N and S containing precursors was also
84 widely detected (Lin et al., 2012b; Sun et al., 2021; Song et al., 2018). The N-containing
85 compounds such as nitroaromatics were important chromophores in HULIS in aged biomass
86 burning organic aerosols (BBOA), as well as in ambient aerosols influenced by biomass burning
87 (BB), while reduced N compounds such as N-heterocyclic aromatic compounds were found to be
88 important chromophores in fresh BBOA (Wang et al., 2019b; Song et al., 2022; Jiang et al., 2020;
89 Wang et al., 2017c). Recent laboratory simulation experiments showed that the photooxidation of
90 various anthropogenic VOCs (e.g., naphthalene, benzene, toluene, and ethylbenzene) would be
91 promoted under high NO_x condition, producing strongly light absorbing nitroaromatics (Yang et
92 al., 2022; Aiona et al., 2018; Siemens et al., 2022; Xie et al., 2017). Otherwise, nighttime oxidation
93 of biogenic or anthropogenic VOCs, such as benzene/toluene, isoprene (C₅H₈) and monoterpenes

94 (C₁₀H₁₆) by NO₃ radicals lead to substantial organonitrates formation, where the VOCs oxidation
95 is strongly affected by NO_x (He et al., 2021; Shen et al., 2021; Wang et al., 2020; Zheng et al.,
96 2021).

97 The organosulfates (OSs) and nitrooxy organosulfates (nitrooxy-OSs) have also been found
98 to widely exist in HULIS in different atmospheric environment (Lin et al., 2012b; Lin et al., 2012a;
99 Sun et al., 2021). Field study and laboratory smog chamber experiments have confirmed that OSs
100 and nitrooxy-OSs in the atmosphere mainly come from the O₃, OH, or NO₃ oxidation of biogenic
101 VOCs such as isoprene, α/β-pinene as well as aromatic hydrocarbon in the presence of H₂SO₄/SO₂
102 (Surratt et al., 2008; Glasius et al., 2021; Yang et al., 2020; Lin et al., 2012b; Huang et al., 2020).
103 Coal combustions were found to be important sources of the aromatic OSs and nitrooxy-OSs in
104 HULIS (Song et al., 2018). Besides, the long-chain alkanes were found to be important precursor
105 of OSs in atmospheric aerosol samples from urban area which was related to vehicle emissions
106 (Wang et al., 2019a; Tao et al., 2014).

107 Nanjing is one of the main cities in the Yangtze River Delta (YRD), which is one of the most
108 developed areas in China. Organic matter can account for 20-40 % of PM_{2.5} in the YRD area due
109 to the impact of complicated sources, especially anthropogenic emissions (Wang et al., 2017a;
110 Wang et al., 2016a). Studies have reported that BrC is an important contributor to aerosol light
111 absorption in Nanjing and exhibited obvious seasonal variations, with peaks in wintertime, owing
112 to emissions from biomass burning, fossil fuel combustion, and secondary formation (Chen et al.,
113 2018; Cui et al., 2021; Xie et al., 2020; Wang et al., 2018a). Recently, works on the field
114 observation of nitrated aromatic compounds (NACs) were conducted to explore the light
115 absorption contributions of NACs to BrC and help to better understand the links between the
116 optical properties and molecular compositions of BrC (Gu et al., 2022; Cao et al., 2023). However,
117 as far as we know, understanding of the sources of atmospheric HULIS at molecular levels was
118 still limited. In this work, the molecular compositions of water soluble HULIS isolated from PM_{2.5}
119 samples collected in summertime and wintertime from 2017 to 2018 at Nanjing, China, were
120 investigated combining the FT-ICR MS and radiocarbon (¹⁴C) analysis. We aim to obtain the
121 molecular characteristic differences of water soluble HULIS in summertime and wintertime and
122 to get a better understanding of the influence of different sources on the molecular compositions
123 of HULIS.

124 **2. Materials and methods**

125 2.1 Sample collection

126 The 24 h PM_{2.5} samples were collected on the roof of Wende building, which was about 21
127 m height from the ground at Nanjing University of Information Science and Technology (32.2° N,
128 118.7° E) using a high-volume sampler (KC-1000, Qingdao, China) at a flow rate of 300 L min⁻¹.
129 The study site was located in the northern suburb area of Nanjing, adjacent to G205 State Road
130 and surrounded by an industrial park and residential area. Generally, the study site was affected
131 by human activity, industrial emission, and traffic emission. The sample collection was conducted
132 in summer from 12 August 2017 to 26 August 2017 and in winter from 31 December 2017 to 31
133 January 2018. A heavy haze event occurred from 31 December 2017 to 3 January 2018, thus the
134 sample frequency was adjusted to 2 h in daytime and 8 h in nighttime. Field blank filters were
135 performed before and after sample collection for each season. More details about the sample
136 collection can be found in previous research reported by Bao et al. (2022). The air pollutants data
137 including PM_{2.5}, SO₂ and NO₂ were provided by China National Environmental Monitoring Centre.
138 Twelve samples were selected for further chemical analysis and the details about the sample
139 selection are described in Section 3.1 in this study.

140 2.2 Chemical analysis

141 The solid phase extraction (SPE) cartridge (Oasis HLB, 30 μm, 60 mg/cartridge, Waters,
142 USA) was performed to isolate the water soluble HULIS in this study. Briefly, the prepared water
143 extracts passed through the pre-conditioned HLB cartridge firstly, then the retained HULIS on the
144 HLB cartridge were eluted with 2% (v/v) ammonia/methanol and evaporated to dryness under a
145 gentle stream of nitrogen gas, then re-dissolved in ultrapure water for the measurement. The carbon
146 fraction in HULIS (HULIS-C) were determined using a total carbon analyzer (Shimadzu-TOC-
147 VCPH, Shimadzu, Japan) with standard deviation of reproducibility test less than 3.5 % and
148 detection limit of 0.14 μg C m⁻³. More details about the HULIS isolation and measurement have
149 been described in Bao et al. (2022).

150 The mass concentrations of the water soluble ions including NO₃⁻, NH₄⁺ and SO₄²⁻ were
151 measured using an ion chromatography (Dionex ICS-5000+, ThermoFisher Scientific, USA)
152 separated on an AS11 column (4*250 mm, Dionex) for anions and a CS12A column
153 (4*250 mm, Dionex) for cations, respectively. Potassium hydroxide (KOH) and methane sulfuric
154 acid (MSA) were used as the gradient eluent for anion and cation determination, respectively. The
155 levoglucosan concentrations were analyzed using the same ion chromatograph equipped with a

156 CarboPac MA1 analytical column (4*250 mm, Dionex) and an electrochemical detector. Sodium
157 hydroxide (NaOH) was used as the gradient eluent for levoglucosan determination. All data were
158 blank corrected in this study. More details of the methods have been described previously (Liu et
159 al., 2019).

160 2.3 Radiocarbon analysis

161 For the radiocarbon measurement of the HULIS samples, the organic solvents were firstly
162 evaporated under a gentle flow of ultrapure N₂ for 30-40 minutes in tin cups. After that, the tin
163 cups were wrapped into balls and more than 50 µg of carbon from the HULIS samples was
164 combusted into CO₂ using an elemental analyzer (EA, model vario micro, elemental, Germany),
165 then reduced into graphite targets for ¹⁴C determination at the State Key Laboratory of Organic
166 Geochemistry, Guangzhou Institute of Geochemistry, Guangzhou, China (Jiang et al., 2020).
167 Detailed descriptions of the ¹⁴C data processing can be found in previous study (Mo et al., 2018).
168 Briefly, the ¹⁴C values were expressed as the modern carbon (f_m) fraction after correcting for the
169 $\delta^{13}\text{C}$ fractionation. The f_m was converted into non-fossil carbon (f_{nf}) fraction with the correction
170 factor of 1.06 ± 0.07 based on the long-term time series of ¹⁴CO₂ sampled at the background station
171 in this study (Levin et al., 2013; Levin and Kromer, 2004). ¹⁴C analysis of the oxalic acid standard
172 (IAEA-C7) was conducted in this study (Xu et al., 2021). No field blank correction was performed
173 for the carbon isotope analysis since the carbon content in the field blanks was negligible.

174 2.4 High-resolution FT-ICR MS analysis

175 The ultrahigh resolution mass spectra of the HULIS samples were obtained through a Solarix
176 XR FT-ICR MS (Bruker Daltonics, GmbH, Bremen, Germany) equipped with a 9.4 T
177 superconducting magnet (Gamry Instruments, Warminster, USA) and a Paracell analyzer cell
178 (Bruker Daltonik GmbH, Bremen, Germany) in the negative ESI mode. The detection mass range
179 was set as m/z 150 to 800 and the ion accumulation time was set as 0.65 s. A total of 100 continuous
180 4M transient data points were superposed to enhance the signal to noise ratio and dynamic range.
181 The mass spectrum was externally calibrated with a standard solution of arginine and internal
182 recalibration was performed using typical O₆S₁ chemical species in DataAnalysis ver. 4.4 software
183 (Bruker Daltonics) (Mo et al., 2018; Tang et al., 2020; Jiang et al., 2020). Field blank filters were
184 analyzed as same as the samples and all the sample data were blank corrected. More details about
185 the data processing can be found in Text S1 in the supporting information.

186 3. Results and discussion

187 3.1 General temporal characteristics during the sampling periods

188 Figure 1 displays the temporal variations of non-fossil contributions to HULIS-C, the mass
189 concentrations of HULIS-C, levoglucosan, NO_3^- , SO_4^{2-} , NH_4^+ , SO_2 , NO_2 , and $\text{PM}_{2.5}$, as well as the
190 relative humidity and temperature during the study periods corresponding to the 12 samples. The
191 12 samples were named as S1-S6 (summer) and W1-W6 (winter) in chronological order
192 corresponding to the six samples in summer and winter, respectively in this study. The averaged
193 mass concentrations of $\text{PM}_{2.5}$ in summer and winter during the selected periods were 21.05 ± 8.05
194 $\mu\text{g m}^{-3}$ and $445.67 \pm 275.00 \mu\text{g m}^{-3}$, respectively, indicating the serious pollution level in winter.
195 The daily $\text{PM}_{2.5}$ mass concentrations in summer were all below the daily averaged Chinese
196 National Ambient Air Quality Standard (NAAQS) of $35 \mu\text{g m}^{-3}$, while the daily $\text{PM}_{2.5}$ mass
197 concentrations in winter all exceeded the daily averaged NAAQS of $35 \mu\text{g m}^{-3}$, of which the $\text{PM}_{2.5}$
198 mass concentrations of W1-W3 and W6 exceeded $200 \mu\text{g m}^{-3}$. The averaged mass concentrations
199 of HULIS in summer and winter during the selected periods were $1.83 \pm 0.27 \mu\text{g m}^{-3}$ and $4.52 \pm$
200 $2.29 \mu\text{g m}^{-3}$, respectively. Compared with those measured in other cities in China in summer, the
201 averaged HULIS concentration in Nanjing in summer was comparable with those measured in
202 Guangzhou of $1.70 \mu\text{g m}^{-3}$ (Fan et al., 2016), Shanghai of $1.61 \mu\text{g m}^{-3}$ (Zhao et al., 2016) and Xi'an
203 of $1.50 \mu\text{g m}^{-3}$ (Zhang et al., 2020b). Compared with those measured in winter samples in other
204 cities, our result was comparable with those in Xi'an of $4.50 \mu\text{g m}^{-3}$ (Zhang et al., 2020b), a little
205 lower than those in the megacity of Shanghai of $5.31 \mu\text{g m}^{-3}$ (Zhao et al., 2016) and higher than
206 those in the southern coastal city of Guangzhou of $3.60 \mu\text{g m}^{-3}$ (Fan et al., 2016).

207 As shown in Fig. 1, the mass concentrations of HULIS-C, levoglucosan, water soluble
208 secondary inorganic aerosols (SIA), and air pollutants showed similar trends in winter, suggesting
209 the influence of BB and anthropogenic emissions in winter (Wu et al., 2019b). The radiocarbon
210 analysis results showed that the f_{nf} of HULIS-C ranged from 30 % to 50 % with an average
211 contribution of 39 ± 8 % in summer and ranged from 32 % to 48 % with an average contribution
212 of 36 ± 6 % in winter, indicating the significant contributions from fossil sources to HULIS at the
213 study site. The 48 h back trajectories (Fig. S1) showed that the study site was affected by the
214 polluted air masses mainly from the northern cities in winter, suggesting the coal combustion
215 contributions to HULIS in winter (Ma et al., 2018; Sun et al., 2021). In addition, significant
216 increasing of the levoglucosan and HULIS-C mass concentrations were found from 31 December
217 2017 to 1 January 2018, corresponding to the W1-W3 samples and the maximum of the

218 levoglucosan and HULIS-C mass concentrations were 552.79 ng m^{-3} and $7.40 \text{ } \mu\text{g m}^{-3}$, respectively,
219 indicating the BB impact during the periods. In summer, the study site was affected by both
220 regional transport from the nearby cities in the north and west of Nanjing and the Donghai Sea.
221 The anthropogenic emissions from the neighboring cities might cause the anthropogenic SOA
222 formation, i.e., secondary N-containing and S-containing compounds with aromatic structures
223 during the atmospheric transport processes, which was discussed in detail in section 3.4 in this
224 study.

225 3.2 Mass spectra and molecular formula assignments

226 Figure S2 and S3 show the negative ion ESI FT-ICR mass spectra of HULIS in summer and
227 winter, respectively. The molecular formulas listed are some of the top ten molecular formulas.
228 Thousands of peaks are present in the spectra in the range from m/z 150 to m/z 600 and the most
229 intense ion peaks are those in the range m/z 200-400 in summer and m/z 150-350 in winter. Our
230 results are similar to those found for the ultrahigh resolution mass spectra of water-soluble organic
231 compounds in particles produced from BB, coal combustion, vehicle exhaust emissions, as well as
232 in ambient aerosols and cloud water samples, within a reasonable range (Tang et al., 2020; Sun et
233 al., 2021; Song et al., 2018; Song et al., 2019; Bianco et al., 2018). In this study, the assigned
234 molecular formulas were classified into the following four main subgroups based on their
235 elemental compositions: CHO (compounds containing only C, H, and O), CHON (compounds
236 containing C, H, O and N), CHOS (compounds containing C, H, O, and S), and CHONS
237 (compounds containing C, H, O, N, and S). As shown in Fig. 2, the proportions of the four
238 subgroups accounted for the overall formulas followed as CHO (20 %-27 %), CHON (28 %-43 %),
239 CHOS (19 %-26 %), and CHONS (16 %-26 %) in summer, respectively and CHO (15 %-19 %),
240 CHON (30 %-40 %), CHOS (21 %-32 %), and CHONS (20 %-29 %) in winter, respectively. The
241 average proportions of the CHO, CHON, CHOS, and CHONS compounds in summer were $22 \pm$
242 3% , $36 \pm 5 \%$, $22 \pm 3 \%$, and $20 \pm 4 \%$, respectively. The average proportions of the four subgroups
243 in winter were $17 \pm 2 \%$, $32 \pm 4 \%$, $24 \pm 3 \%$, and $27 \pm 4 \%$, respectively. The CHON groups were
244 the major components of molecular formulas, furthermore, the relative intensity of CHON groups
245 increased significantly in winter (Fig. S2 and Fig. S3). Studies have suggested that HULIS emitted
246 from biomass burning can produce a high abundance of CHON compounds and S-containing
247 compounds were the dominant component for primary HULIS emitted from coal combustion
248 (Zhang et al., 2021; Song et al., 2018). The higher intensity of CHON compounds in winter in this

249 study further indicated the BB contribution. The contributions of S-containing compounds (CHOS
250 and CHONS groups) increased in winter which might be related to the polluted air masses
251 transported from the northern cities with increasing coal combustions emissions in winter (Song
252 et al., 2018). Notably, the relatively higher proportions of CHO and CHON groups in summer
253 were most probably related to the increasing biogenic emissions in summer, resulting in the
254 formation of some high molecular weight oligomers or highly oxidized organonitrates, which was
255 discussed in detail in section 3.4.1 and 3.4.2 in this study.

256 Table S1 and S2 displays the composition characteristics of atmospheric HULIS in the
257 summer and winter samples, including the relative intensity weighted average values of number,
258 molecular weight (MW_w), elemental ratios (O/C_w and H/C_w), double-bond equivalent (DBE_w),
259 aromaticity index (AI_w), and DBE/C_w . A total of 14387 and 15731 peaks were detected in the
260 summer and winter samples, respectively. The O/C and H/C ratios are commonly calculated to
261 evaluate the oxidation degree and saturation degree of the compounds, respectively (Ning et al.,
262 2022). The O/C_w values were in a range of 0.61-0.80 with an average value of 0.71 ± 0.07 for
263 summer samples and in a range of 0.59-0.67 with an average value of 0.62 ± 0.03 for winter
264 samples, respectively. The higher oxidation degree of summer samples than winter samples
265 indicated stronger secondary HULIS formation in summer. The H/C_w values were in a range of
266 1.38-1.46 with an average value of 1.42 ± 0.03 for summer samples and in a range of 1.33-1.41
267 with an average value of 1.36 ± 0.04 for winter samples, respectively. The O/C_w and H/C_w of each
268 molecular subgroup followed a changing trend of $CHO < CHON < CHOS < CHONS$ compounds.
269 Most of the S-containing compounds had a O/C value ≥ 0.7 , suggesting the large amounts of highly
270 oxidized OSs in S-containing compounds which contained various functional groups and were
271 mainly from the photochemical oxidation of biogenic or anthropogenic volatile organic
272 compounds (VOCs) (Mutzel et al., 2015). The DBE values were calculated to describe the degree
273 of unsaturation of compounds and restricted the assigned molecular formulas with unreasonably
274 high or low number of rings or double bonds (Kroll et al., 2011). The related parameter DBE/C
275 was the double-bond equivalent of unit carbon which can reflect the condensed ring structures in
276 the compounds (Jiang et al., 2021). The higher DBE_w and DBE/C_w values of CHO and CHON
277 compounds were found in this study, indicating the higher unsaturation degree of these two groups.

278 Considering that double bonds can be formed by heteroatoms especially O atoms, whereas
279 make no contributions to the aromaticity of the compounds, AI_w was calculated to supplement the

280 DBE results (Song et al., 2018; Ning et al., 2019). AI_w can eliminate the contribution of O, N, and
281 S atoms to the C=C double bond density of molecules. The AI_w values of different compounds
282 groups in HULIS presented the changing trends: $AI_w(\text{CHONS}) > AI_w(\text{CHON}) > AI_w(\text{CHO}) >$
283 $AI_w(\text{CHOS})$ in summer and $AI_w(\text{CHON}) > AI_w(\text{CHO}) > AI_w(\text{CHONS}) > AI_w(\text{CHOS})$ in winter,
284 respectively. The formulas can be classified into three parts based on AI values proposed by
285 previous studies: aliphatic ($AI=0$), olefinic ($0 < AI \leq 0.5$) and aromatic ($AI > 0.5$) (Koch and Dittmar,
286 2006; Jiang et al., 2020; Ning et al., 2019). As shown in Fig. S4 and S5, the aliphatic were the
287 main components of S-containing compounds in this study and the olefinic and aromatic were the
288 main components of CHO and CHON compounds. Furthermore, the aromatic proportion of CHO
289 and CHON compounds significantly increased in winter, suggesting the increasing anthropogenic
290 emissions in winter.

291 3.3 Comparative analysis using Van Krevelen diagrams

292 In this study, the Van Krevelen diagrams (Fig. 3) were constructed to display the molecular
293 composition and categorical distribution of the collected samples (Noziere et al., 2015; Patriarca
294 et al., 2018; Li et al., 2022). According to the elemental ratios (O/C and H/C ratios) and AI values,
295 seven major compound classes were classified, including lipids-like species, lignins-like species,
296 proteins-like species, tannins-like species, carbohydrates-like species, condensed aromatics
297 structure, and unsaturated hydrocarbons (Table S3). The Van Krevelen diagrams showed similar
298 distributions in the 12 samples. The CHO and CHON compounds located in the lower left area
299 and the S-containing compounds located in the upper light area with higher O/C and H/C ratios,
300 indicating a higher degree of oxidation and saturation. The condensed aromatic structure mainly
301 consisted in the CHO and CHON compounds, further suggesting the influence of anthropogenic
302 emissions on the formation of CHO and CHON compounds.

303 Figure 4 presents the averaged relative contributions of the number of molecular formulas
304 from the seven categories in summer and winter samples, respectively. Lignins-like species
305 accounted for the highest proportion of CHO compounds with average contributions of 58 % and
306 61 % in summer and winter, respectively, followed by CHON compounds with average
307 contributions of 48 % and 57 % in summer and winter, respectively. Lignins are mainly composed
308 of carboxyl groups, alicyclic rings, aromatic rings, and other O-containing groups. Previous studies
309 have reported that lignin was a complex phenolic polymer which usually came from direct
310 biological emissions or combustions of biofuel (Ning et al., 2019; Boreddy et al., 2021; Sun et al.,

311 2021). Lignins pyrolysis products and other lignins derived molecules have been shown to be
312 oxidized into light absorbing BrC chromophore under certain conditions (Fleming et al., 2020).

313 Tannins-like species accounted for 21 %, 27 %, 23 %, and 30 % of CHO, CHON, CHOS, and
314 CHONS compounds, respectively in summer which were higher than those in winter with
315 contributions of 13 %, 16 %, 16 %, and 23 % to CHO, CHON, CHOS, and CHONS compounds,
316 respectively. Tannins-like species are a series of polyphenolic compounds containing hydroxyls
317 and carboxylic groups which have been widely reported in fogs, cloud water and aerosol samples,
318 attributing to highly oxidized organic compounds such as OSs or nitrooxy-OSs produced from the
319 nighttime chemistry between the biogenic VOCs with the NO₃ (Altieri et al., 2009; Bianco et al.,
320 2018; Ning et al., 2019; Altieri et al., 2008; Shen et al., 2021). Carbohydrates-like species which
321 contain monosaccharide, alditols, and anhydrosugars mainly consisted in CHONS compounds
322 which also had a relative higher proportion of 33 % in summer than that of 29 % in winter (Sun et
323 al., 2021). C₁₀H₁₆NO₇₋₉S, as monoterpene nitrooxy-OSs, showing high relative intensities, were
324 typical carbohydrates-like species detected in this study which represented biogenic secondary
325 organic aerosols (SOA) (Ning et al., 2019; Surratt et al., 2008; Wang et al., 2020). Both the higher
326 proportions of tannins-like and carbohydrates-like classes in summer indicated stronger biogenic
327 SOA formation in this study.

328 Proteins-like classes mainly consisted in CHOS compounds with average proportions of 29 %
329 and 38 % in summer and winter, respectively. Proteins contain peptide-like structures formed by
330 dehydration with different kinds of amino acids and consist of short chains of amino acid residues
331 (Bianco et al., 2018). These compounds are associated with photochemical oxidation processing
332 in aerosols, thus resulting in the significant formation of OSs from biogenic or anthropogenic
333 precursors in this study (Bigg and Leck, 2008).

334 Higher condensed aromatics were detected in winter with average proportions of 14 % in
335 CHO compounds and 8 % in CHON compounds, respectively which were 2-2.5 times of those in
336 summer. Condensed aromatics are important components of PAHs which were usually emitted
337 from incomplete combustion of fossil fuels (Ma et al., 2020). The increase of the proportion of
338 condensed aromatics in winter indicated the stronger influence of anthropogenic sources on
339 HULIS formation. The unsaturated hydrocarbons and lipids-like species showed the lowest
340 molecular number percentage of less than 1 % in this study. Previous studies have shown that the

341 lipids-like species were the main components of water insoluble organic compounds in aerosols
342 and could be attributed to monocarboxylic acids (Ning et al., 2022; Wozniak et al., 2008).

343 In summary, both the summer and winter samples were mainly composed of compounds from
344 biogenic origins (lignins-like, tannins-like, proteins-like, and carbohydrates-like species). More
345 tannins-like and carbohydrates-like species were detected in summer including large amounts of
346 highly oxidized OSs or nitrooxy-OSs, indicating biogenic SOA formation. More condensed
347 aromatic structures in CHO and CHON compounds were detected in winter, owing to increasing
348 anthropogenic emissions. It is noted that ESI ionization technology is more sensitive for the
349 identification of polar compounds (Jiang et al., 2014; Lin et al., 2018). Therefore, the low polar or
350 nonpolar compounds, such as PAHs or their derivatives from fossil sources, were probably
351 underestimated in this study.

352 3.4 Molecular composition of HULIS

353 3.4.1 Molecular characteristics of CHO compounds

354 The O/C_w and H/C_w ratios for the CHO compounds were 0.45-0.56 and 1.15-1.30 for the
355 summer samples and 0.42-0.48 and 0.90-1.02 for the winter samples (Table S1 and S2). The
356 summer samples showed higher oxidation degree and saturation degree. We firstly plotted the Van
357 Krevelen diagrams of the four molecular subgroups showing relative intensities for all the 12
358 samples and similar distributions of the high-intensity compounds were found in the 6 summer
359 samples and the 6 winter samples, respectively. Then we combined all the data in summer and
360 winter, respectively. As shown in Fig. 5a and 5d, the CHO compounds in summer with high
361 relative abundance were located at the area within $0.2 \leq O/C \leq 1.0$ and $1.0 \leq H/C \leq 1.7$, mainly
362 including lignins-like species and tannins-like species which were closely related to biogenic
363 emissions. On the contrary, the condensed aromatics showed high relative abundance in winter,
364 suggesting obviously different sources of HULIS in summer and winter. The DBE values
365 increased with the increasing of the C numbers (Fig. 5b and 5e). The high-intensity CHO
366 compounds in HULIS had DBE values between 3-7 with C numbers from 10 to 20 for summer
367 samples. In winter, the high-intensity CHO compounds had DBE values between 7-11 with C
368 numbers from 5 to 15. As mentioned above, the aromatic ($AI > 0.5$) proportion of CHO compounds
369 significantly increased in winter, the higher DBE values in winter further indicated the consists of
370 more highly unsaturated aromatic compounds which reflected the anthropogenic emissions.

371 The CHO compounds were classified according to the number of oxygen atoms to evaluate
372 the oxygen content. As shown in Fig. 5c and 5f, the high-intensity CHO compounds with 6-11
373 oxygen atom were detected in summer, such as $C_{15}H_{24}O_6$, $C_{15}H_{22}O_{10}$, $C_{18}H_{26}O_8$, and $C_{18}H_{26}O_9$,
374 these highly oxygenated organic molecules with high molecular weight have also been detected in
375 laboratory α -pinene ozonolysis SOA (Pospisilova et al., 2020). We further classified the CHO
376 compounds by different carbon atom numbers. As shown in Fig. S6, the C_{17} - C_{22} compounds were
377 the main components of the CHO compounds, accounting for more than 50 % of the total number
378 of CHO molecular formulas in both summer and winter seasons. However, the total relative
379 intensities of the CHO compounds in summer were significantly higher than those in winter, of
380 which the C_{23} - C_{26} and C_{27} - C_{32} compounds were enriched in summer. These high molecular weight
381 compounds were probably oligomers formed from various biogenic precursors, such as isoprene,
382 sesquiterpene, and monoterpene (Daellenbach et al., 2019; Berndt et al., 2018). The high intensities
383 of these compounds in summer further indicated the stronger biogenic SOA formation in summer
384 compared with that in winter.

385 High-intensity CHO compounds with 4-9 oxygen atom were detected in winter (Fig. 5c) of
386 which the $C_{14}H_{10}O_4$ formula with a DBE value of 10 appeared the highest intensity, which was
387 probable functional PAHs and have been reported in HULIS from coal combustion smoke particles
388 (Song et al., 2019). As shown in Fig. S2 and S3, the $C_{14}H_{10}O_4$ formula appeared high intensity in
389 all the winter samples, providing the evidence of coal combustion emissions in winter. Some other
390 high-intensity compounds in winter, such as $C_{14}H_8O_4$ and $C_{14}H_8O_5$ both with DBE values of 11,
391 and $C_{13}H_8O_2$, $C_{13}H_8O_5$, and $C_{13}H_8O_6$ with DBE values of 10, might refer to hydroxyl substitutions
392 derived from anthracenedione and xanthone, respectively, which have been reported in secondary
393 wood combustion products (Bruns et al., 2015). $C_{15}H_{10}O_6$, $C_{15}H_8O_6$, and $C_{16}H_{12}O_7$ which had
394 DBE values of 11, 12, and 11, respectively, might be flavonoids which had flavone backbone, the
395 key structure of plant pigments, widely existing in plants in nature and could be important sources
396 of BrC chromophores in aged BBOA (Fleming et al., 2020; Lin et al., 2016; Huang et al., 2021).
397 Phenolic substances derived from phenol, guaiacol, and syringol are also widely existed in BBOA,
398 usually from the pyrolysis of lignins in wood, which also play an important role in aqueous-phase
399 SOA formation (Boreddy et al., 2021). For instance, $C_{13}H_{10}O_3$ and $C_{13}H_{10}O_5$ are guaiacol
400 derivatives, $C_{15}H_{16}O_8$ are syringol derivatives and $C_{18}H_{14}O_6$ and $C_{18}H_{14}O_7$ are phenol derivatives
401 (Sun et al., 2021). As shown in Fig. S7, the relative intensities of the CHO compounds mentioned

402 above produced from BB were found to have similar trends with the mass concentrations of
403 levoglucosan, which were significantly higher in W1-W3 samples, corresponding to the BB period
404 from 31 December 2017 to 1 January 2018, providing the evidence of BB influence on HULIS
405 formation in winter.

406 It is noted that the top compounds $C_9H_6O_7$ and $C_{10}H_6O_8$ were detected both in the summer
407 and winter samples (Fig. S2 and S3), which had DBE values of 7 and 8, respectively, containing
408 abundant condensed aromatic ring structures with high O numbers. Their peaks were also detected
409 in the HFO (heavy-fuel-oil)-fueled off-road engine samples reported before, suggesting the traffic
410 emission contributions to HULIS (Cui et al., 2019). This supported the radiocarbon analysis results
411 in this study and gave further information that the traffic emissions were important fossil sources
412 in both summer and winter seasons, which was also found in previous research which reported the
413 sources of HULIS based on the positive matrix factorization (PMF) model by Bao et al. (2022).

414 3.4.2 Molecular characteristics of CHON compounds

415 The O/C_w of CHON compounds in summer and winter were 0.57-0.71 and 0.52-0.56,
416 respectively, while the H/C_w were 1.20-1.32 and 1.00-1.11, respectively (Table S1 and S2).
417 Compared with the summer CHON compounds, the winter CHON compounds presented
418 significantly higher ion abundance (Fig. 6a and 6d). The most abundant CHON subgroups had
419 DBE values of 4-7 and 3-10 in summer and winter, respectively (Fig. 6b and 6e). Similar with the
420 CHO compounds, the higher DBE values of high-intensity CHON compounds in HULIS in winter
421 indicated a high prevalence of double bonds or ring structures. According to the N and O number,
422 the CHON compounds were classified into N_1O_x (N_1O_1 - N_1O_{15}) and N_2O_x (N_2O_2 - N_2O_{14}) subgroups
423 in summer and N_1O_x (N_1O_1 - N_1O_{12}) and N_2O_x (N_2O_2 - N_2O_{12}) subgroups in winter, respectively (Fig.
424 6c and 6f). NO_{8-12} and NO_{6-9} compounds were mostly enriched subgroups in summer and winter,
425 respectively. More oxygen-enriched CHON compounds containing O number above 9 were
426 detected in summer, implying the higher oxidation degree for summer samples. In addition, the
427 N_1O_x were both the major compounds represented average of $64 \pm 4 \%$ and $61 \pm 6 \%$ of the CHON
428 molecular formulas in summer and winter, respectively, indicating the presence of more single
429 nitro/amino substituents in CHON compounds in this study.

430 Among the CHON compounds, $95 \pm 1 \%$ and $86 \pm 3 \%$ CHON compounds had O/N values
431 ≥ 3 in summer and winter, respectively in this study, indicating these compounds contained large
432 amounts of oxidized nitrogen functional groups such as nitro compounds ($-NO_2$) and/or

433 organonitrates (-ONO₂) and excess oxygen atoms indicated the existence of other oxygen-
434 containing functional groups (Laskin et al., 2009). The organonitrates formation from NO₃
435 oxidation of biogenic or anthropogenic VOCs can affect the interactions between anthropogenic
436 and natural emissions (He et al., 2021; Shen et al., 2021; Wang et al., 2020). Organonitrates were
437 found to be important species contributing to SOA formation in the polluted urban environment,
438 which were enhanced under high NO_x level (Zheng et al., 2021). The significant higher relative
439 intensities of CHON compounds in winter indicated that the high NO_x environment in winter
440 promoted the formation of organonitrates and highlighted the importance of organonitrates for SOA
441 control in polluted environment.

442 Furthermore, we found that the increase of the relative abundance of CHON compounds in
443 winter was particularly significant in W1-W3 samples (Fig. S2 and S3), corresponding to the BB
444 episode. Phenols produced from the pyrolysis of lignins can react with NO₃ radicals in the
445 atmosphere, producing nitrophenols, which have been shown to be important BrC chromophore
446 in BBOA (Wang et al., 2017c; Lin et al., 2016; Cai et al., 2020). It was reported that the gas-phase
447 reactions of NO₃ radicals with phenolic substances took place at least 4 orders of magnitude faster
448 than those with aromatic hydrocarbon and even faster in the aqueous phase (Lin et al., 2017).
449 Among the top CHON compounds with high relative abundance in W1-W3 samples, such as
450 C₆H₄N₂O₆ and C₇H₆N₂O₆ both with a DBE value of 6, were refer to nitrophenols containing one
451 or two nitrogen-containing functional groups, which have been widely reported in aged BBOA,
452 indicating the increasing of the CHON compounds relative intensity in W1-W3 samples were
453 closely related to BB (Lin et al., 2017; Cai et al., 2020; Mohr et al., 2013; Kourtchev et al., 2016;
454 Lin et al., 2016). Some other top CHON compounds in winter samples such as C₉H₄NO₄ and
455 C₁₀H₆NO₄ with low O/C and H/C ratios most likely indicated the presence of condensed aromatic
456 structures in the compounds. The C₉H₄NO₄ compounds were most likely emitted from vehicle
457 emissions which have previously been reported (Cui et al., 2019).

458 It is worth noting that some high-intensity CHON compounds with low O/C and H/C ratios
459 were detected in summer samples in this study (Fig. 6a), which were closely related to aromatic
460 compounds from anthropogenic emissions. The top compounds with molecular formulas of
461 C₈H₅N₂O₂ and C₁₉H₁₁N₂O₄, which had O/N of 1 and 2, respectively, were both reduced N
462 compounds referring to N-heterocyclic compounds. Previously studies have found that the N-
463 heterocyclic aromatic compounds can be formed through the aldehyde–ammonia reactions (De

464 Haan et al., 2018; Zhang et al., 2022a). This indicated the important role of reduced N species (e.g.,
465 ammonium) in the formation of anthropogenic SOA in summer. Our results were consistent with
466 previous study conducted in Xi'an, China which also found formation of reduced N compounds in
467 light-absorbing aerosols through ammonia involved reactions in summer (Zeng et al., 2021).

468 3.4.3 Molecular characteristics of S-containing compounds (CHOS and CHONS compounds)

469 The O/C_w of CHOS compounds in summer and winter were 0.60-0.79 and 0.56-0.67,
470 respectively, while the H/C_w were 1.50-1.54 and 1.53-1.72, respectively. The O/C_w of CHONS
471 compounds in summer and winter were 0.82-1.01 and 0.76-0.94, respectively, while the H/C_w
472 were 1.57-1.65 and 1.58-1.66, respectively (Table S1 and S2). As shown in Fig. 7a, 7d, 8a, and 8d,
473 the high-intensity S-containing compounds in summer and winter were both located at the area
474 where $O/C > 0.5$ and $H/C > 1.5$, respectively. In addition, the relative intensity of S-containing
475 compounds increased with the O/C ratios, suggesting the S-containing compounds were highly
476 oxidized. A small number of high-intensity S-containing compounds with $O/C < 1.0$ and $H/C < 1.0$
477 were also found in winter in this study, which might be related to OSs and nitrooxy-OSs produced
478 from the oxidation of aromatic hydrocarbon. The CHOS compounds presenting high relative
479 abundance were rich in $O_{6-9}S$ and $O_{5-7}S$ groups in summer and winter, respectively, of which the
480 DBE values were all below 4. The CHONS compounds were rich in $O_{8-10}S$ and $O_{7-9}S$ groups in
481 summer and winter, respectively, of which the DBE values were all below 6 (Fig. 7b, 7e, 7c, 7f,
482 8b, 8e, 8c, and 8f). Compared with those of the CHO and CHON compounds, the DBE values of
483 S-containing compounds were significantly lower.

484 Among the S-containing compounds, more than 95 % of the CHOS, $CHON_1S$, and $CHON_2S$
485 formulas had O/S ratios greater than 4, 7, and 10, respectively, implying these compounds may
486 contain organic sulfate functional groups ($-OSO_3$) or one or two organic nitrate groups ($-ONO_2$)
487 and these compounds were more likely OSs or nitrooxy-OSs, presenting lower DBE values and
488 higher O/C and H/C ratios (Table S5 and S6) (O'Brien et al., 2014). The high-intensity CHONS
489 compounds observed in this study, such as $C_{10}H_{16}NO_{7-9}S$, $C_{10}H_{18}NO_{8-9}S$, $C_{10}H_{18}N_2O_{11}S$, and
490 $C_9H_{14}NO_{8-9}S$ could be nitrooxy-OSs derived from monoterpenes such as limonene and α -terpinene
491 of which we found the formulas in summer contained more oxygen atoms, indicating the higher
492 oxidation degree of these nitrooxy-OSs in summer (Figure S2 and S3) (Sun et al., 2021;
493 Bruggemann et al., 2020; Wang et al., 2020; Wang et al., 2018d).

494 The CHOS compounds with high intensity abundance, such as typical isoprene epoxydiols
495 (IEPOX) derived OSs with molecular formulas of $C_5H_8O_7S$ and $C_5H_{10}O_7S$ were both detected in
496 the summer and winter samples, of which the relative intensity of $C_5H_8O_7S$ were over 80 % in S1,
497 S2, S5, and S6 samples, indicating the significant isoprene SOA formation in summer (Kourtchev
498 et al., 2016; Kourtchev et al., 2013). The results were consistent with the PMF results reported by
499 Bao et al. (2022). The monoterpenes derived OSs such as $C_8H_{14}O_6S$, $C_8H_{14}O_8S$, $C_{10}H_{18}O_8$,
500 $C_{10}H_{14}O_6$, and $C_{11}H_{16}O_7$ were detected in both summer and winter samples in this study, which
501 could refer to monoterpene-OSs derived from α -pinene, α -terpinene, and limonene (Wang et al.,
502 2020). Moreover, OSs with high carbon numbers ($C \geq 14$) such as $C_{14}H_{22}O_7S$, $C_{14}H_{22}O_8S$,
503 $C_{14}H_{24}O_7S$, $C_{15}H_{26}O_7S$, $C_{15}H_{24}O_7S$, $C_{15}H_{24}O_8S$, and $C_{16}H_{28}O_7S$ were also observed in both
504 summer and winter samples. Long-chain alkanes emitted from vehicle emissions might be
505 precursors of these OSs which was consistent with the molecular structures of OSs collected in
506 urban areas affected by traffic emissions such as Shanghai, Los Angeles, and Beijing (Wang et al.,
507 2019a; Tao et al., 2014; Wang et al., 2016b). The aromatic OSs such as naphthalene derived OSs
508 with molecular formulas of $C_{10}H_{10}O_6S$, $C_{10}H_{10}O_7S$, and $C_{10}H_{12}O_7S$, 2-methylnaphthalene derived
509 OSs with molecular formulas of $C_9H_{12}O_6S$, $C_{11}H_{12}O_7S$, and $C_{11}H_{14}O_7S$, and hydroxybenzene
510 derived OSs with molecular formulas of $C_6H_6O_5S$ were also observed in this study (Qi et al., 2021;
511 Riva et al., 2015; Blair et al., 2017). Figure S8 further displays the ternary plot of the relative
512 intensities of OSs from biogenic precursors (e.g., isoprene and monoterpenes), long-chain alkanes
513 and aromatic hydrocarbon. As shown in Fig. S8, the biogenic OSs and long-chain alkanes OSs
514 formation were comparable in summer and winter, demonstrating both biogenic and anthropogenic
515 emission contributions to HULIS. The aromatic OSs presented higher relative intensities in winter,
516 further indicating the increasing anthropogenic emissions in winter. The presence of long-chain
517 alkanes derived OSs in both summer and winter seasons provided another evidence that the traffic
518 emission was one of the important fossil sources of HULIS in this study.

519 3.5 Comparison with organic compounds in source and atmospheric aerosol samples

520 The O/C and H/C ratios of water soluble HULIS in this study were compared with those of
521 water soluble organic compounds reported in source samples from BB, coal combustions, and
522 vehicle emissions (Tang et al., 2020; Song et al., 2018; Cui et al., 2019; Song et al., 2019), cloud
523 water samples (Bianco et al., 2018; Zhao et al., 2013), rainwater samples (Altieri et al., 2009) and
524 fog samples (Brege et al., 2018) (Fig. 9). In addition, the O/C and H/C ratios of organic fraction in

525 aerosol samples collected in Beijing (Jang et al., 2020; Wu et al., 2019a; Wang et al., 2018a),
526 Tianjin (Han et al., 2022), Baoding (Sun et al., 2021), Shanghai (Wang et al., 2017b), Guangzhou
527 (Jiang et al., 2021), respectively in China, Mainz (Wang et al., 2018b), Cork city (Kourtchev et al.,
528 2014), and Bologna (Brege et al., 2018), respectively in Europe, and Bakersfield (O'Brien et al.,
529 2014) and Virginia (Willoughby et al., 2014), respectively in the United States were also shown
530 in Fig. 9. The O/C ratios were obviously higher than those detected in primary BB, coal
531 combustion, and vehicle emission samples. The H/C ratios of the CHO and CHON compounds
532 were comparable with the source samples, indicating the organics in HULIS experienced
533 atmospheric secondary process and the mixed sources of HULIS in this study. The H/C ratios of
534 the S-containing compounds were much higher than those of source samples which could be
535 attributed to the significant organosulfates formation in the atmosphere.

536 The O/C ratios reported in this study were also higher than those reported in aerosol samples
537 in urban area in China, further indicating the serious secondary pollution at Nanjing, China.
538 Among the CHO and CHON compounds, we found that the highest H/C ratio values were observed
539 in the southern city of Guangzhou, followed by those in Nanjing and Shanghai, and the lowest
540 values were observed in the northern cities such as Beijing, Tianjin, and Baoding, indicating the
541 higher unsaturation degree of the aerosol samples collected from the northern cities, which were
542 also considered as the heavy industrial region in China. The higher H/C ratios of aerosol samples
543 collected in Europe and the United States indicated the less anthropogenic emissions such as
544 industrial emissions from those areas.

545 **4. Conclusions**

546 This study focuses on the sources and molecular characteristics differences of water soluble
547 HULIS in summertime and wintertime from 2017 to 2018 at a suburb site of the YRD, China based
548 on the radiocarbon analysis and FT-ICR MS measurement with ESI ion source in negative mode.
549 The carbon isotope analysis results highlight the important fossil source contributions to HULIS
550 at the study site. A total of 14387 and 15731 peaks were detected in the summer and winter samples,
551 respectively based on the FT-ICR MS results. The assigned molecular formulas were classified
552 into CHO, CHON, CHOS, and CHONS subgroups according to their elemental compositions. The
553 Van Krevelen diagrams showed that more tannins-like and carbohydrates-like species were
554 detected in summer indicating biogenic SOA formation. Whereas more compounds containing
555 condensed aromatic structures were detected in winter which were derived from anthropogenic

556 emissions. The total relative intensity of CHO compounds in summer were significantly higher
557 than those in winter, containing lots of macromolecular oligomers derived from biogenic
558 precursors. The high-intensity CHO compounds in winter were mainly aromatic compounds such
559 as phenolic substances and flavonoids which were related to aged BBOA and oxidized PAHs most
560 probably from fossil fuel combustion. On the contrary, the total relative intensity of CHON
561 compounds significantly increased in winter, mainly composed of nitro compounds or
562 organonitrates. The enhanced formation of nitrophenols in winter indicated the BB influence. The
563 increasing organonitrates formation in winter highlighted the secondary N-containing compounds
564 formation via NO₃ radical-initiated oxidation processes. It is worth noting that the top CHON
565 compounds in summer were referring to aromatic reduced N compounds produced from the
566 aldehyde–ammonia reactions. The S-containing compounds were mainly composed of highly
567 oxidized OSs. The monoterpenes derived OSs and long-chain alkanes derived OSs were widely
568 observed in both summer and winter samples, while the aromatic OSs formation were found to be
569 more significant in winter. The presence of long-chain alkanes derived OSs supported the
570 radiocarbon results, indicating that the traffic emission was the important fossil sources at the study
571 site. The presence of aromatic secondary N-containing and S-containing compounds provided
572 evidence for the substantial contributions from anthropogenic SOA formation to fossil sources at
573 the study site. These results further verified the work reported before by Bao et al. (2022) based
574 on the PMF model which have found the significant anthropogenic SOA and fossil fuel
575 combustion contributions to HULIS in urban area in China at molecular level. In addition, strong
576 biogenic emission in summer and BB in winter were found in this study, highlighting the
577 importance of different control policies for each season in the future.

578

579 **Acknowledgments**

580 This research was financially supported by the National Natural Science Foundation of China
581 (grant no. 42192512) and the National Natural Science Foundation of China (grant no. 41977305).

582

583 **References**

584 Aiona, P. K., Luek, J. L., Timko, S. A., Powers, L. C., Gonsior, M., and Nizkorodov, S. A.: Effect
585 of photolysis on absorption and fluorescence spectra of light-absorbing secondary organic aerosols,
586 *Acc. Earth. Space. Chem.*, 2, 235-245, 10.1021/acsearthspacechem.7b00153, 2018.

587 Altieri, K. E., Seitzinger, S. P., Carlton, A. G., Turpin, B. J., Klein, G. C., and Marshall, A. G.:
588 Oligomers formed through in-cloud methylglyoxal reactions: Chemical composition, properties,
589 and mechanisms investigated by ultra-high resolution FT-ICR mass spectrometry, *Atmos.*
590 *Environ.*, 42, 1476-1490, 10.1016/j.atmosenv.2007.11.015, 2008.

591 Altieri, K. E., Turpin, B. J., and Seitzinger, S. P.: Oligomers, organosulfates, and nitrooxy
592 organosulfates in rainwater identified by ultra-high resolution electrospray ionization FT-ICR
593 mass spectrometry, *Atmos. Chem. Phys.*, 9, 2533–2542, www.atmos-chem-phys.net/9/2533/2009/
594 2009.

595 Bao, M., Zhang, Y. L., Cao, F., Lin, Y. C., Hong, Y., Fan, M., Zhang, Y., Yang, X., and Xie, F.:
596 Light absorption and source apportionment of water soluble humic-like substances (HULIS) in
597 PM_{2.5} at Nanjing, China, *Environ. Res.*, 206, 112554, 10.1016/j.envres.2021.112554, 2022.

598 Berndt, T., Mender, B., Scholz, W., Fischer, L., Herrmann, H., Kulmala, M., and Hansel, A.:
599 Accretion product formation from ozonolysis and OH radical reaction of alpha-Pinene:
600 mechanistic insight and the influence of isoprene and ethylene, *Environ. Sci. Technol.*, 52, 11069-
601 11077, 10.1021/acs.est.8b02210, 2018.

602 Bianco, A., Deguillaume, L., Vaitilingom, M., Nicol, E., Baray, J. L., Chaumerliac, N., and
603 Bridoux, M.: Molecular characterization of cloud water samples collected at the Puy de Dome
604 (France) by Fourier transform ion cyclotron resonance mass spectrometry, *Environ. Sci. Technol.*,
605 52, 10275-10285, 10.1021/acs.est.8b01964, 2018.

606 Bigg, E. K., and Leck, C.: The composition of fragments of bubbles bursting at the ocean surface,
607 *J. Geophys. Res.*, 113, 10.1029/2007jd009078, 2008.

608 Blair, S. L., MacMillan, A. C., Drozd, G. T., Goldstein, A. H., Chu, R. K., Pasa-Tolic, L., Shaw,
609 J. B., Tolic, N., Lin, P., Laskin, J., Laskin, A., and Nizkorodov, S. A.: Molecular characterization
610 of organosulfur compounds in biodiesel and diesel fuel secondary organic aerosol, *Environ. Sci.*
611 *Technol.*, 51, 119-127, 10.1021/acs.est.6b03304, 2017.

612 Boreddy, S. K. R., Hegde, P., Aswini, A. R., and Aryasree, S.: Chemical characteristics, size
613 distributions, molecular composition, and brown carbon in South Asian outflow to the Indian
614 Ocean, *Earth. Space. Sci.*, 8, 10.1029/2020ea001615, 2021.

615 Brege, M., Paglione, M., Gilardoni, S., Decesari, S., Facchini, M. C., and Mazzoleni, L. R.:
616 Molecular insights on aging and aqueous-phase processing from ambient biomass burning

617 emissions-influenced Po Valley fog and aerosol, *Atmos. Chem. Phys.*, 18, 13197-13214,
618 10.5194/acp-18-13197-2018, 2018.

619 Bruggemann, M., Xu, R., Tilgner, A., Kwong, K. C., Mutzel, A., Poon, H. Y., Otto, T., Schaefer,
620 T., Poulain, L., Chan, M. N., and Herrmann, H.: Organosulfates in ambient aerosol: state of
621 knowledge and future research directions on formation, abundance, fate, and importance, *Environ.*
622 *Sci. Technol.*, 54, 3767-3782, 10.1021/acs.est.9b06751, 2020.

623 Bruns, E. A., Krapf, M., Orasche, J., Huang, Y., Zimmermann, R., Drinovec, L., Močnik, G., El-
624 Haddad, I., Slowik, J. G., Dommen, J., Baltensperger, U., and Prévôt, A. S. H.: Characterization
625 of primary and secondary wood combustion products generated under different burner loads,
626 *Atmos. Chem. Phys.*, 15, 2825-2841, 10.5194/acp-15-2825-2015, 2015.

627 Cai, J., Zeng, X., Zhi, G., Gligorovski, S., Sheng, G., Yu, Z., Wang, X., and Peng, P. a.: Molecular
628 composition and photochemical evolution of water-soluble organic carbon (WSOC) extracted
629 from field biomass burning aerosols using high-resolution mass spectrometry, *Atmos. Chem.*
630 *Phys.*, 20, 6115-6128, 10.5194/acp-20-6115-2020, 2020.

631 Cao, M., Yu, W., Chen, M., and Chen, M.: Characterization of nitrated aromatic compounds in
632 fine particles from Nanjing, China: Optical properties, source allocation, and secondary processes,
633 *Environ. Pollut.*, 316, 120650, 10.1016/j.envpol.2022.120650, 2023.

634 Chen, Q., Ikemori, F., Higo, H., Asakawa, D., and Mochida, M.: Chemical structural
635 characteristics of HULIS and other fractionated organic matter in urban aerosols: results from mass
636 spectral and FT-IR analysis, *Environ. Sci. Technol.*, 50, 1721-1730, 10.1021/acs.est.5b05277,
637 2016.

638 Chen, Y., Ge, X., Chen, H., Xie, X., Chen, Y., Wang, J., Ye, Z., Bao, M., Zhang, Y., and Chen,
639 M.: Seasonal light absorption properties of water-soluble brown carbon in atmospheric fine
640 particles in Nanjing, China, *Atmos. Environ.*, 187, 230-240, 10.1016/j.atmosenv.2018.06.002,
641 2018.

642 Chung, C. E., Ramanathan, V., and Decremier, D.: Observationally constrained estimates of
643 carbonaceous aerosol radiative forcing, *Proc. Natl. Acad. Sci. U. S. A.*, 109, 11624-11629,
644 10.1073/pnas.1203707109, 2012.

645 Cui, F., Pei, S., Chen, M., Ma, Y., and Pan, Q.: Absorption enhancement of black carbon and the
646 contribution of brown carbon to light absorption in the summer of Nanjing, China, *Atmos. Pollut.*
647 *Res.*, 12, 480-487, 10.1016/j.apr.2020.12.008, 2021.

648 Cui, M., Li, C., Chen, Y., Zhang, F., Li, J., Jiang, B., Mo, Y., Li, J., Yan, C., Zheng, M., Xie, Z.,
649 Zhang, G., and Zheng, J.: Molecular characterization of polar organic aerosol constituents in off-
650 road engine emissions using Fourier transform ion cyclotron resonance mass spectrometry (FT-
651 ICR MS): implications for source apportionment, *Atmos. Chem. Phys.*, 19, 13945-13956,
652 10.5194/acp-19-13945-2019, 2019.

653 Daellenbach, K. R., Kourtchev, I., Vogel, A. L., Bruns, E. A., Jiang, J., Petäjä, T., Jaffrezo, J.-L.,
654 Aksoyoglu, S., Kalberer, M., Baltensperger, U., El Haddad, I., and Prévôt, A. S. H.: Impact of
655 anthropogenic and biogenic sources on the seasonal variation in the molecular composition of
656 urban organic aerosols: a field and laboratory study using ultra-high-resolution mass spectrometry,
657 *Atmos. Chem. Phys.*, 19, 5973-5991, 10.5194/acp-19-5973-2019, 2019.

658 De Haan, D. O., Tapavicza, E., Riva, M., Cui, T., Surratt, J. D., Smith, A. C., Jordan, M. C.,
659 Nilakantan, S., Almodovar, M., Stewart, T. N., de Loera, A., De Haan, A. C., Cazaunau, M.,
660 Gratien, A., Pangui, E., and Doussin, J. F.: Nitrogen-containing, light-Absorbing oligomers
661 produced in aerosol particles exposed to methylglyoxal, photolysis, and cloud cycling, *Environ.*
662 *Sci. Technol.*, 52, 4061-4071, 10.1021/acs.est.7b06105, 2018.

663 Fan, X., Song, J., and Peng, P. a.: Temporal variations of the abundance and optical properties of
664 water soluble Humic-Like Substances (HULIS) in PM_{2.5} at Guangzhou, China, *Atmos. Res.*, 172-
665 173, 8-15, 10.1016/j.atmosres.2015.12.024, 2016.

666 Fleming, L. T., Lin, P., Roberts, J. M., Selimovic, V., Yokelson, R., Laskin, J., Laskin, A., and
667 Nizkorodov, S. A.: Molecular composition and photochemical lifetimes of brown carbon
668 chromophores in biomass burning organic aerosol, *Atmos. Chem. Phys.*, 20, 1105-1129,
669 10.5194/acp-20-1105-2020, 2020.

670 Gu, C., Cui, S., Ge, X., Wang, Z., Chen, M., Qian, Z., Liu, Z., Wang, X., and Zhang, Y.: Chemical
671 composition, sources and optical properties of nitrated aromatic compounds in fine particulate
672 matter during winter foggy days in Nanjing, China, *Environ. Res.*, 212, 113255,
673 10.1016/j.envres.2022.113255, 2022.

674 Glasius, M., Thomsen, D., Wang, K., Iversen, L. S., Duan, J., and Huang, R. J.: Chemical
675 characteristics and sources of organosulfates, organosulfonates, and carboxylic acids in aerosols
676 in urban Xi'an, Northwest China, *Sci. Total. Environ.*, 151187, 10.1016/j.scitotenv.2021.151187,
677 2021.

678 Graber, E. R., and Rudich, Y.: Atmospheric HULIS: How humic-like are they? A comprehensive
679 and critical review, *Atmos. Chem. Phys.*, 6, 729-753, 10.5194/acp-6-729-2006, 2006.

680 Han, H., Feng, Y., Chen, J., Xie, Q., Chen, S., Sheng, M., Zhong, S., Wei, W., Su, S., and Fu, P.:
681 Acidification impacts on the molecular composition of dissolved organic matter revealed by FT-
682 ICR MS, *Sci. Total. Environ.*, 805, 150284, 10.1016/j.scitotenv.2021.150284, 2022.

683 He, Q., Tomaz, S., Li, C., Zhu, M., Meidan, D., Riva, M., Laskin, A., Brown, S. S., George, C.,
684 Wang, X., and Rudich, Y.: Optical properties of secondary organic aerosol produced by nitrate
685 radical oxidation of biogenic volatile organic compounds, *Environ. Sci. Technol.*, 55, 2878-2889,
686 10.1021/acs.est.0c06838, 2021.

687 Huang, L., Liu, T., and Grassian, V. H.: Radical-initiated formation of aromatic organosulfates
688 and sulfonates in the aqueous phase, *Environ. Sci. Technol.*, 54, 11857-11864,
689 10.1021/acs.est.0c05644, 2020.

690 Huang, R.-J., Yang, L., Shen, J., Yuan, W., Gong, Y., Ni, H., Duan, J., Yan, J., Huang, H., You,
691 Q., and Li, Y. J.: Chromophoric fingerprinting of brown carbon from residential biomass burning,
692 *Environ. Sci. Technol. Lett.*, 9, 102-111, 10.1021/acs.estlett.1c00837, 2021.

693 Huo, Y., Guo, Z., Li, Q., Wu, D., Ding, X., Liu, A., Huang, D., Qiu, G., Wu, M., Zhao, Z., Sun,
694 H., Song, W., Li, X., Chen, Y., Wu, T., and Chen, J.: Chemical fingerprinting of HULIS in
695 particulate matters emitted from residential coal and biomass combustion, *Environ. Sci. Technol.*,
696 55, 3593-3603, 10.1021/acs.est.0c08518, 2021.

697 Jang, K. S., Choi, M., Park, M., Park, M. H., Kim, Y. H., Seo, J., Wang, Y., Hu, M., Bae, M. S.,
698 and Park, K.: Assessment of PM_{2.5}-bound nitrogen-containing organic compounds (NOCs) during
699 winter at urban sites in China and Korea, *Environ. Pollut.*, 265, 114870,
700 10.1016/j.envpol.2020.114870, 2020.

701 Jiang, B., Liang, Y., Xu, C., Zhang, J., Hu, M., and Shi, Q.: Polycyclic aromatic hydrocarbons
702 (PAHs) in ambient aerosols from Beijing: characterization of low volatile PAHs by positive-ion
703 atmospheric pressure photoionization (APPI) coupled with Fourier transform ion cyclotron
704 resonance, *Environ. Sci. Technol.*, 48, 4716-4723, 10.1021/es405295p, 2014.

705 Jiang, H., Li, J., Chen, D., Tang, J., Cheng, Z., Mo, Y., Su, T., Tian, C., Jiang, B., Liao, Y., and
706 Zhang, G.: Biomass burning organic aerosols significantly influence the light absorption properties
707 of polarity-dependent organic compounds in the Pearl River Delta Region, China, *Environ. Int.*,
708 144, 106079, 10.1016/j.envint.2020.106079, 2020.

709 Jiang, H., Li, J., Sun, R., Tian, C., Tang, J., Jiang, B., Liao, Y., Chen, C. E., and Zhang, G.:
710 Molecular dynamics and light absorption properties of atmospheric dissolved organic matter,
711 *Environ. Sci. Technol.*, **55**, 10268-10279, 10.1021/acs.est.1c01770, 2021.

712 Koch, B. P., and Dittmar, T.: From mass to structure: an aromaticity index for high-resolution
713 mass data of natural organic matter, *Rapid. Commun. Mass. Sp.*, **20**, 926-932, 10.1002/rcm.2386,
714 2006.

715 Kourtchev, I., Fuller, S., Aalto, J., Ruuskanen, T. M., McLeod, M. W., Maenhaut, W., Jones, R.,
716 Kulmala, M., and Kalberer, M.: Molecular composition of boreal forest aerosol from Hyytiälä,
717 Finland, using ultrahigh resolution mass spectrometry, *Environ. Sci. Technol.*, **47**, 4069-4079,
718 10.1021/es3051636, 2013.

719 Kourtchev, I., O'Connor, I. P., Giorio, C., Fuller, S. J., Kristensen, K., Maenhaut, W., Wenger, J.
720 C., Sodeau, J. R., Glasius, M., and Kalberer, M.: Effects of anthropogenic emissions on the
721 molecular composition of urban organic aerosols: An ultrahigh resolution mass spectrometry study,
722 *Atmos. Environ.*, **89**, 525-532, 10.1016/j.atmosenv.2014.02.051, 2014.

723 Kourtchev, I., Godoi, R. H. M., Connors, S., Levine, J. G., Archibald, A. T., Godoi, A. F. L.,
724 Paralovo, S. L., Barbosa, C. G. G., Souza, R. A. F., Manzi, A. O., Seco, R., Sjostedt, S., Park, J.-
725 H., Guenther, A., Kim, S., Smith, J., Martin, S. T., and Kalberer, M.: Molecular composition of
726 organic aerosols in central Amazonia: an ultra-high-resolution mass spectrometry study, *Atmos.*
727 *Chem. Phys.*, **16**, 11899-11913, 10.5194/acp-16-11899-2016, 2016.

728 Kroll, J. H., Donahue, N. M., Jimenez, J. L., Kessler, S. H., Canagaratna, M. R., Wilson, K. R.,
729 Altieri, K. E., Mazzoleni, L. R., Wozniak, A. S., Bluhm, H., Mysak, E. R., Smith, J. D., Kolb, C.
730 E., and Worsnop, D. R.: Carbon oxidation state as a metric for describing the chemistry of
731 atmospheric organic aerosol, *Nat. Chem.*, **3**, 133-139, 10.1038/nchem.948, 2011.

732 Kuang, B. Y., Lin, P., Huang, X. H. H., and Yu, J. Z.: Sources of humic-like substances in the
733 Pearl River Delta, China: positive matrix factorization analysis of PM_{2.5} major components and
734 source markers, *Atmos. Chem. Phys.*, **15**, 1995-2008, 10.5194/acp-15-1995-2015, 2015.

735 Laskin, A., Smith, J. S., and Laskin, J.: Molecular characterization of nitrogen-containing organic
736 compounds in biomass burning aerosols using high-resolution mass spectrometry, *Environ. Sci.*
737 *Technol.*, **43**, 3764-3771, 10.1021/es803456n, 2009.

738 Laskin, J., Laskin, A., and Nizkorodov, S. A.: Mass spectrometry analysis in atmospheric
739 chemistry, *Anal. Chem.*, **90**, 166-189, 10.1021/acs.analchem.7b04249, 2018.

740 Levin, I., and Kromer, B.: The tropospheric $^{14}\text{CO}_2$ level in mid-latitudes of the northern
741 hemisphere (1959–2003), *Radiocarbon*, 46, 1261-1272, 10.1017/s0033822200033130, 2004.

742 Levin, I., Kromer, B., and Hammer, S.: Atmospheric $\Delta^{14}\text{CO}_2$ trend in Western European
743 background air from 2000 to 2012, *Tellus. B.*, 65, 10.3402/tellusb.v65i0.20092, 2013.

744 Li, X., Han, J., Hopke, P. K., Hu, J., Shu, Q., Chang, Q., and Ying, Q.: Quantifying primary and
745 secondary humic-like substances in urban aerosol based on emission source characterization and
746 a source-oriented air quality model, *Atmos. Chem. Phys.*, 19, 2327-2341, 10.5194/acp-19-2327-
747 2019, 2019.

748 Li, X., Yu, F., Cao, J., Fu, P., Hua, X., Chen, Q., Li, J., Guan, D., Tripathee, L., Chen, Q., and
749 Wang, Y.: Chromophoric dissolved organic carbon cycle and its molecular compositions and
750 optical properties in precipitation in the Guanzhong basin, China, *Sci. Total. Environ.*, 814, 152775,
751 10.1016/j.scitotenv.2021.152775, 2022.

752 Lin, P., Rincon, A. G., Kalberer, M., and Yu, J. Z.: Elemental composition of HULIS in the Pearl
753 River Delta Region, China: results inferred from positive and negative electrospray high resolution
754 mass spectrometric data, *Environ. Sci. Technol.*, 46, 7454-7462, 10.1021/es300285d, 2012a.

755 Lin, P., Yu, J. Z., Engling, G., and Kalberer, M.: Organosulfates in humic-like substance fraction
756 isolated from aerosols at seven locations in East Asia: a study by ultra-high-resolution mass
757 spectrometry, *Environ. Sci. Technol.*, 46, 13118-13127, 10.1021/es303570v, 2012b.

758 Lin, P., Aiona, P. K., Li, Y., Shiraiwa, M., Laskin, J., Nizkorodov, S. A., and Laskin, A.: Molecular
759 characterization of brown carbon in biomass burning aerosol particles, *Environ. Sci. Technol.*, 50,
760 11815-11824, 10.1021/acs.est.6b03024, 2016.

761 Lin, P., Bluvshstein, N., Rudich, Y., Nizkorodov, S. A., Laskin, J., and Laskin, A.: Molecular
762 chemistry of atmospheric brown carbon inferred from a nationwide biomass burning event,
763 *Environ. Sci. Technol.*, 51, 11561-11570, 10.1021/acs.est.7b02276, 2017.

764 Lin, P., Fleming, L. T., Nizkorodov, S. A., Laskin, J., and Laskin, A.: Comprehensive molecular
765 characterization of atmospheric brown carbon by high resolution mass spectrometry with
766 electrospray and atmospheric pressure photoionization, *Anal. Chem.*, 90, 12493-12502,
767 10.1021/acs.analchem.8b02177, 2018.

768 Liu, X., Zhang, Y.-L., Peng, Y., Xu, L., Zhu, C., Cao, F., Zhai, X., Haque, M. M., Yang, C., Chang,
769 Y., Huang, T., Xu, Z., Bao, M., Zhang, W., Fan, M., and Lee, X.: Chemical and optical properties

770 of carbonaceous aerosols in Nanjing, eastern China: regionally transported biomass burning
771 contribution, *Atmos. Chem. Phys.*, 19, 11213-11233, 10.5194/acp-19-11213-2019, 2019.

772 Ma, L., Li, B., Liu, Y., Sun, X., Fu, D., Sun, S., Thapa, S., Geng, J., Qi, H., Zhang, A., and Tian,
773 C.: Characterization, sources and risk assessment of PM_{2.5}-bound polycyclic aromatic
774 hydrocarbons (PAHs) and nitrated PAHs (NPAHs) in Harbin, a cold city in Northern China, *J.*
775 *Clean. Prod.*, 264, 10.1016/j.jclepro.2020.121673, 2020.

776 Ma, Y., Cheng, Y., Qiu, X., Cao, G., Fang, Y., Wang, J., Zhu, T., Yu, J., and Hu, D.: Sources and
777 oxidative potential of water-soluble humic-like substances (HULIS_{WS}) in fine particulate matter
778 (PM_{2.5}) in Beijing, *Atmos. Chem. Phys.*, 18, 5607-5617, 10.5194/acp-18-5607-2018, 2018.

779 Mo, Y., Li, J., Jiang, B., Su, T., Geng, X., Liu, J., Jiang, H., Shen, C., Ding, P., Zhong, G., Cheng,
780 Z., Liao, Y., Tian, C., Chen, Y., and Zhang, G.: Sources, compositions, and optical properties of
781 humic-like substances in Beijing during the 2014 APEC summit: Results from dual carbon isotope
782 and Fourier-transform ion cyclotron resonance mass spectrometry analyses, *Environ. Pollut.*, 239,
783 322-331, 10.1016/j.envpol.2018.04.041, 2018.

784 Mohr, C., Lopez-Hilfiker, F. D., Zotter, P., Prevot, A. S., Xu, L., Ng, N. L., Herndon, S. C.,
785 Williams, L. R., Franklin, J. P., Zahniser, M. S., Worsnop, D. R., Knighton, W. B., Aiken, A. C.,
786 Gorkowski, K. J., Dubey, M. K., Allan, J. D., and Thornton, J. A.: Contribution of nitrated phenols
787 to wood burning brown carbon light absorption in Detling, United Kingdom during winter time,
788 *Environ. Sci. Technol.*, 47, 6316-6324, 10.1021/es400683v, 2013.

789 Mutzel, A., Poulain, L., Berndt, T., Iinuma, Y., Rodigast, M., Boge, O., Richters, S., Spindler, G.,
790 Sipila, M., Jokinen, T., Kulmala, M., and Herrmann, H.: Highly oxidized multifunctional organic
791 compounds observed in tropospheric particles: a field and laboratory study, *Environ. Sci. Technol.*,
792 49, 7754-7761, 10.1021/acs.est.5b00885, 2015.

793 Ning, C., Gao, Y., Zhang, H., Yu, H., Wang, L., Geng, N., Cao, R., and Chen, J.: Molecular
794 characterization of dissolved organic matters in winter atmospheric fine particulate matters (PM_{2.5})
795 from a coastal city of northeast China, *Sci. Total. Environ.*, 689, 312-321,
796 10.1016/j.scitotenv.2019.06.418, 2019.

797 Ning, C., Gao, Y., Yu, H., Zhang, H., Geng, N., Cao, R., and Chen, J.: FT-ICR mass spectrometry
798 for molecular characterization of water-insoluble organic compounds in winter atmospheric fine
799 particulate matters, *J. Environ. Sci.*, 111, 51-60, 10.1016/j.jes.2020.12.017, 2022.

800 Noziere, B., Kalberer, M., Claeys, M., Allan, J., D'Anna, B., Decesari, S., Finessi, E., Glasius, M.,
801 Grgic, I., Hamilton, J. F., Hoffmann, T., Iinuma, Y., Jaoui, M., Kahnt, A., Kampf, C. J., Kourtev,
802 I., Maenhaut, W., Marsden, N., Saarikoski, S., Schnelle-Kreis, J., Surratt, J. D., Szidat, S.,
803 Szmigielski, R., and Wisthaler, A.: The molecular identification of organic compounds in the
804 atmosphere: state of the art and challenges, *Chem. Rev.*, 115, 3919-3983, 10.1021/cr5003485,
805 2015.

806 O'Brien, R. E., Laskin, A., Laskin, J., Rubitschun, C. L., Surratt, J. D., and Goldstein, A. H.:
807 Molecular characterization of S- and N-containing organic constituents in ambient aerosols by
808 negative ion mode high-resolution Nanospray desorption electrospray ionization mass
809 spectrometry: CalNex 2010 field study, *J. Geophys. Res. -Atmos.*, 119, 10.1002/2014jd021955,
810 2014.

811 Patriarca, C., Bergquist, J., Sjoberg, P. J. R., Tranvik, L., and Hawkes, J. A.: Online HPLC-ESI-
812 HRMS method for the analysis and comparison of different dissolved organic matter samples,
813 *Environ. Sci. Technol.*, 52, 2091-2099, 10.1021/acs.est.7b04508, 2018.

814 Pospisilova, V., Lopez-Hilfiker, F. D., Bell, D. M., Haddad, I. E., Mohr, C., Huang, W., Heikkinen,
815 L., Xiao, M., Dommen, J., Prevot, A. S. H., Baltensperger, U., and Slowik, J. G.: On the fate of
816 oxygenated organic molecules in atmospheric aerosol particles, *Sci. Adv.*, 6, 2020.

817 Qi, L., Zhang, Z., Wang, X., Deng, F., Zhao, J., and Liu, H.: Molecular characterization of
818 atmospheric particulate organosulfates in a port environment using ultrahigh resolution mass
819 spectrometry: Identification of traffic emissions, *J. Hazard. Mater.*, 419, 126431,
820 10.1016/j.jhazmat.2021.126431, 2021.

821 Riva, M., Tomaz, S., Cui, T., Lin, Y.-H., Perraudin, E., Gold, A., Stone, E. A., Villenave, E., and
822 Surratt, J. D.: Evidence for an unrecognized secondary anthropogenic source of organosulfates and
823 sulfonates: gas-phase oxidation of polycyclic aromatic hydrocarbons in the presence of sulfate
824 aerosol, *Environ. Sci. Technol.*, 49, 6654-6664, 10.1021/acs.est.5b00836, 2015.

825 Shen, H., Zhao, D., Pullinen, I., Kang, S., Vereecken, L., Fuchs, H., Acir, I. H., Tillmann, R.,
826 Rohrer, F., Wildt, J., Kiendler-Scharr, A., Wahner, A., and Mentel, T. F.: Highly oxygenated
827 organic nitrates formed from NO₃ radical-initiated oxidation of beta-Pinene, *Environ. Sci.*
828 *Technol.*, 10.1021/acs.est.1c03978, 2021.

829 Siemens, K., Morales, A., He, Q., Li, C., Hettiyadura, A. P. S., Rudich, Y., and Laskin, A.:
830 Molecular analysis of secondary brown carbon produced from the photooxidation of naphthalene,
831 *Environ. Sci. Technol.*, 2022.

832 Song, J., Li, M., Jiang, B., Wei, S., Fan, X., and Peng, P.: Molecular characterization of water-
833 soluble humic like substances in smoke particles emitted from combustion of biomass materials
834 and coal using Ultrahigh-resolution electrospray ionization fourier transform ion cyclotron
835 resonance mass spectrometry, *Environ. Sci. Technol.*, 52, 2575-2585, 10.1021/acs.est.7b06126,
836 2018.

837 Song, J., Li, M., Fan, X., Zou, C., Zhu, M., Jiang, B., Yu, Z., Jia, W., Liao, Y., and Peng, P.:
838 Molecular characterization of water- and methanol-soluble organic compounds emitted from
839 residential coal combustion using Ultrahigh-resolution electrospray ionization fourier transform
840 ion cyclotron resonance mass spectrometry, *Environ. Sci. Technol.*, 53, 13607-13617,
841 10.1021/acs.est.9b04331, 2019.

842 Song, J., Li, M., Zou, C., Cao, T., Fan, X., Jiang, B., Yu, Z., Jia, W., and Peng, P.: Molecular
843 characterization of nitrogen-containing compounds in humic-like substances emitted from
844 biomass burning and coal combustion, *Environ. Sci. Technol.*, 56, 119-130,
845 10.1021/acs.est.1c04451, 2022.

846 Sun, H., Li, X., Zhu, C., Huo, Y., Zhu, Z., Wei, Y., Yao, L., Xiao, H., and Chen, J.: Molecular
847 composition and optical property of humic-like substances (HULIS) in winter-time PM_{2.5} in the
848 rural area of North China Plain, *Atmos. Environ.*, 252, 10.1016/j.atmosenv.2021.118316, 2021.

849 Surratt, J. D., Gómez-González, Y., Chan, A. W. H., Vermeylen, R., Shahgholi, M., Kleindienst,
850 T. E., Edney, E. O., Offenberg, J. H., Lewandowski, M., Jaoui, M., Maenhaut, W., Claeys, M.,
851 Flagan, R. C., and Seinfeld, J. H.: Organosulfate formation in biogenic secondary organic aerosol,
852 *J. Phys. Chem. A* 112, 8345-8378, 10.1021/jp802310p, 2008.

853 Tang, J., Li, J., Su, T., Han, Y., Mo, Y., Jiang, H., Cui, M., Jiang, B., Chen, Y., Tang, J., Song, J.,
854 Peng, P. a., and Zhang, G.: Molecular compositions and optical properties of dissolved brown
855 carbon in biomass burning, coal combustion, and vehicle emission aerosols illuminated by
856 excitation–emission matrix spectroscopy and Fourier transform ion cyclotron resonance mass
857 spectrometry analysis, *Atmos. Chem. Phys.*, 20, 2513-2532, 10.5194/acp-20-2513-2020, 2020.

858 Tao, S., Lu, X., Levac, N., Bateman, A. P., Nguyen, T. B., Bones, D. L., Nizkorodov, S. A., Laskin,
859 J., Laskin, A., and Yang, X.: Molecular characterization of organosulfates in organic aerosols from

860 Shanghai and Los Angeles urban areas by nanospray-desorption electrospray ionization high-
861 resolution mass spectrometry, *Environ. Sci. Technol.*, 48, 10993-11001, 10.1021/es5024674, 2014.

862 Tsui, W. G., and McNeill, V. F.: Modeling secondary organic aerosol production from
863 photosensitized humic-like substances (HULIS), *Environ. Sci. Technol. Lett.*, 5, 255-259,
864 10.1021/acs.estlett.8b00101, 2018.

865 Wang, J., Ge, X., Chen, Y., Shen, Y., Zhang, Q., Sun, Y., Xu, J., Ge, S., Yu, H., and Chen, M.:
866 Highly time-resolved urban aerosol characteristics during springtime in Yangtze River Delta,
867 China: insights from soot particle aerosol mass spectrometry, *Atmos. Chem. Phys.*, 16, 9109–9127,
868 <https://doi.org/10.5194/acp-16-9109-2016>, 2016a.

869 Wang, J., Nie, W., Cheng, Y., Shen, Y., Chi, X., Wang, J., Huang, X., Xie, Y., Sun, P., Xu, Z., Qi,
870 X., Su, H., and Ding, A.: Light absorption of brown carbon in eastern China based on 3-year multi-
871 wavelength aerosol optical property observations and an improved absorption Ångström exponent
872 segregation method, *Atmos. Chem. Phys.*, 18, 9061-9074, 10.5194/acp-18-9061-2018, 2018a.

873 Wang, J., Zhao, B., Wang, S., Yang, F., Xing, J., Morawska, L., Ding, A., Kulmala, M., Kerminen,
874 V.-M., Kujansuu, J., Wang, Z., Ding, D., Zhang, X., Wang, H., Tian, M., Petäjä, T., Jiang, J., and
875 Hao, J.: Particulate matter pollution over China and the effects of control policies, *Sci. Total*
876 *Environ.*, 584–585, 426–447, <https://doi.org/10.1016/j.scitotenv.2017.01.027>, 2017a.

877 Wang, K., Zhang, Y., Huang, R.-J., Cao, J., and Hoffmann, T.: UHPLC-Orbitrap mass
878 spectrometric characterization of organic aerosol from a central European city (Mainz, Germany)
879 and a Chinese megacity (Beijing), *Atmos. Environ.*, 189, 22-29, 10.1016/j.atmosenv.2018.06.036,
880 2018b.

881 Wang, K., Zhang, Y., Huang, R. J., Wang, M., Ni, H., Kampf, C. J., Cheng, Y., Bilde, M., Glasius,
882 M., and Hoffmann, T.: Molecular characterization and source identification of atmospheric
883 particulate organosulfates using ultrahigh resolution mass spectrometry, *Environ. Sci. Technol.*,
884 53, 6192-6202, 10.1021/acs.est.9b02628, 2019a.

885 Wang, X., Hayeck, N., Brüggemann, M., Yao, L., Chen, H., Zhang, C., Emmelin, C., Chen, J.,
886 George, C., and Wang, L.: Chemical characteristics of organic aerosols in Shanghai: a Study by
887 Ultrahigh-performance liquid chromatography coupled with orbitrap mass spectrometry, *J.*
888 *Geophys. Res. -Atmos.*, 122, 11,703-711,722, 10.1002/2017jd026930, 2017b.

889 Wang, X., Heald, C. L., Liu, J., Weber, R. J., Campuzano-Jost, P., Jimenez, J. L., Schwarz, J. P.,
890 and Perring, A. E.: Exploring the observational constraints on the simulation of brown carbon,
891 *Atmos. Chem. Phys.*, 18, 635-653, 10.5194/acp-18-635-2018, 2018c.

892 Wang, X. K., Rossignol, S., Ma, Y., Yao, L., Wang, M. Y., Chen, J. M., George, C., and Wang,
893 L.: Molecular characterization of atmospheric particulate organosulfates in three megacities at the
894 middle and lower reaches of the Yangtze River, *Atmos. Chem. Phys.*, 16, 2285-2298, 10.5194/acp-
895 16-2285-2016, 2016b.

896 Wang, Y., Hu, M., Lin, P., Guo, Q., Wu, Z., Li, M., Zeng, L., Song, Y., Zeng, L., Wu, Y., Guo, S.,
897 Huang, X., and He, L.: Molecular characterization of nitrogen-containing organic compounds in
898 humic-like substances emitted from straw residue burning, *Environ. Sci. Technol.*, 51, 5951-5961,
899 10.1021/acs.est.7b00248, 2017c.

900 Wang, Y., Hu, M., Guo, S., Wang, Y., Zheng, J., Yang, Y., Zhu, W., Tang, R., Li, X., Liu, Y., Le
901 Breton, M., Du, Z., Shang, D., Wu, Y., Wu, Z., Song, Y., Lou, S., Hallquist, M., and Yu, J.: The
902 secondary formation of organosulfates under interactions between biogenic emissions and
903 anthropogenic pollutants in summer in Beijing, *Atmos. Chem. Phys.*, 18, 10693-10713,
904 10.5194/acp-18-10693-2018, 2018d.

905 Wang, Y., Hu, M., Lin, P., Tan, T., Li, M., Xu, N., Zheng, J., Du, Z., Qin, Y., Wu, Y., Lu, S., Song,
906 Y., Wu, Z., Guo, S., Zeng, L., Huang, X., and He, L.: Enhancement in particulate organic nitrogen
907 and light absorption of humic-like substances over Tibetan Plateau due to long-range transported
908 biomass burning emissions, *Environ. Sci. Technol.*, 53, 14222-14232, 10.1021/acs.est.9b06152,
909 2019b.

910 Wang, Y., Hu, M., Wang, Y.-C., Li, X., Fang, X., Tang, R., Lu, S., Wu, Y., Guo, S., Wu, Z.,
911 Hallquist, M., and Yu, J. Z.: Comparative study of particulate organosulfates in contrasting
912 atmospheric environments: field evidence for the significant influence of anthropogenic sulfate
913 and NO_x, *Environ. Sci. Technol. Lett.*, 7, 787-794, 10.1021/acs.estlett.0c00550, 2020.

914 Willoughby, A. S., Wozniak, A. S., and Hatcher, P. G.: A molecular-level approach for
915 characterizing water-insoluble components of ambient organic aerosol particulates using
916 ultrahigh-resolution mass spectrometry, *Atmos. Chem. Phys.*, 14, 10299-10314, 10.5194/acp-14-
917 10299-2014, 2014.

918 Wozniak, A. S., Bauer, J. E., Sleighter, R. L., Dickhut, R. M., and Hatcher, P. G.: Technical note:
919 Molecular characterization of aerosol-derived water soluble organic carbon using ultrahigh

920 resolution electrospray ionization Fourier transform ion cyclotron resonance mass spectrometry,
921 *Atmos. Chem. Phys.*, 8, 5099–5111, www.atmos-chem-phys.net/8/5099/2008/, 2008.

922 Wu, C., Yang, J., Fu, Q., Zhu, B., Ruan, T., and Jiang, G.: Molecular characterization of water-
923 soluble organic compounds in PM_{2.5} using ultrahigh resolution mass spectrometry, *Sci. Total*
924 *Environ.*, 668, 917-924, [10.1016/j.scitotenv.2019.03.031](https://doi.org/10.1016/j.scitotenv.2019.03.031), 2019a.

925 Wu, G., Ram, K., Fu, P., Wang, W., Zhang, Y., Liu, X., Stone, E. A., Pradhan, B. B., Dangol, P.
926 M., Panday, A. K., Wan, X., Bai, Z., Kang, S., Zhang, Q., and Cong, Z.: Water-soluble brown
927 carbon in atmospheric aerosols from Godavari (Nepal), a regional representative of South Asia,
928 *Environ. Sci. Technol.*, 53, 3471-3479, [10.1021/acs.est.9b00596](https://doi.org/10.1021/acs.est.9b00596), 2019b.

929 Xu, B., Cheng, Z., Gustafsson, Ö., Kawamura, K., Jin, B., Zhu, S., Tang, T., Zhang, B., Li, J., and
930 Zhang, G.: Compound-specific radiocarbon analysis of low molecular weight dicarboxylic acids
931 in ambient aerosols using preparative gas chromatography: method development, *Environ. Sci.*
932 *Technol. Lett.*, 8, 135-141, [10.1021/acs.estlett.0c00887](https://doi.org/10.1021/acs.estlett.0c00887), 2021.

933 Xie, M., Chen, X., Hays, M. D., Lewandowski, M., Offenberg, J., Kleindienst, T. E., and Holder,
934 A. L.: Light absorption of secondary organic aerosol: composition and contribution of
935 nitroaromatic compounds, *Environ. Sci. Technol.*, 51, 11607-11616, [10.1021/acs.est.7b03263](https://doi.org/10.1021/acs.est.7b03263),
936 2017.

937 Xie, X., Chen, Y., Nie, D., Liu, Y., Liu, Y., Lei, R., Zhao, X., Li, H., and Ge, X.: Light-absorbing
938 and fluorescent properties of atmospheric brown carbon: A case study in Nanjing, China,
939 *Chemosphere*, 251, 126350, [10.1016/j.chemosphere.2020.126350](https://doi.org/10.1016/j.chemosphere.2020.126350), 2020.

940 Yang, Z., Tsona, N. T., Li, J., Wang, S., Xu, L., You, B., and Du, L.: Effects of NO_x and SO₂ on
941 the secondary organic aerosol formation from the photooxidation of 1,3,5-trimethylbenzene: A
942 new source of organosulfates, *Environ. Pollut.*, 264, 114742, [10.1016/j.envpol.2020.114742](https://doi.org/10.1016/j.envpol.2020.114742), 2020.

943 Yang, Z., Tsona, N. T., George, C., and Du, L.: Nitrogen-containing compounds enhance Light
944 absorption of aromatic-derived brown carbon, *Environ. Sci. Technol.*, [10.1021/acs.est.1c08794](https://doi.org/10.1021/acs.est.1c08794),
945 2022.

946 Zeng, Y., Ning, Y., Shen, Z., Zhang, L., Zhang, T., Lei, Y., Zhang, Q., Li, G., Xu, H., Ho, S. S.
947 H., and Cao, J.: The roles of N, S, and O in molecular absorption features of brown carbon in PM_{2.5}
948 in a typical semi-arid megacity in Northwestern China, *J. Geophys. Res: Atmospheres*, 126,
949 [10.1029/2021jd034791](https://doi.org/10.1029/2021jd034791), 2021.

950 Zhang, A., Wang, Y., Zhang, Y., Weber, R. J., Song, Y., Ke, Z., and Zou, Y.: Modeling the global
951 radiative effect of brown carbon: a potentially larger heating source in the tropical free troposphere
952 than black carbon, *Atmos. Chem. Phys.*, 20, 1901-1920, 10.5194/acp-20-1901-2020, 2020a.

953 Zhang, R., Gen, M., Liang, Z., Li, Y. J., and Chan, C. K.: Photochemical reactions of glyoxal
954 during particulate ammonium nitrate photolysis: brown carbon formation, enhanced glyoxal decay,
955 and organic phase formation, *Environ. Sci. Technol.*, 56, 1605-1614, 10.1021/acs.est.1c07211,
956 2022a.

957 Zhang, T., Shen, Z., Zhang, L., Tang, Z., Zhang, Q., Chen, Q., Lei, Y., Zeng, Y., Xu, H., and Cao,
958 J.: PM_{2.5} Humic-like substances over Xi'an, China: Optical properties, chemical functional group,
959 and source identification, *Atmos. Res.*, 234, 10.1016/j.atmosres.2019.104784, 2020b.

960 Zhang, T., Shen, Z., Zeng, Y., Cheng, C., Wang, D., Zhang, Q., Lei, Y., Zhang, Y., Sun, J., Xu,
961 H., Ho, S. S. H., and Cao, J.: Light absorption properties and molecular profiles of HULIS in PM_{2.5}
962 emitted from biomass burning in traditional "Heated Kang" in Northwest China, *Sci. Total.
963 Environ.*, 776, 146014, 10.1016/j.scitotenv.2021.146014, 2021.

964 Zhang, T., Huang, S., Wang, D., Sun, J., Zhang, Q., Xu, H., Hang Ho, S. S., Cao, J., and Shen, Z.:
965 Seasonal and diurnal variation of PM_{2.5} HULIS over Xi'an in Northwest China: Optical properties,
966 chemical functional group, and relationship with reactive oxygen species (ROS), *Atmos. Environ.*,
967 268, 118782, <https://doi.org/10.1016/j.atmosenv.2021.118782>, 2022b.

968 Zhang, T., Shen, Z., Huang, S., Lei, Y., Zeng, Y., Sun, J., Zhang, Q., Ho, S. S. H., Xu, H., and
969 Cao, J.: Optical properties, molecular characterizations, and oxidative potentials of different
970 polarity levels of water-soluble organic matters in winter PM_{2.5} in six China's megacities, *Sci.
971 Total. Environ.*, 853, 158600, <https://doi.org/10.1016/j.scitotenv.2022.158600>, 2022c.

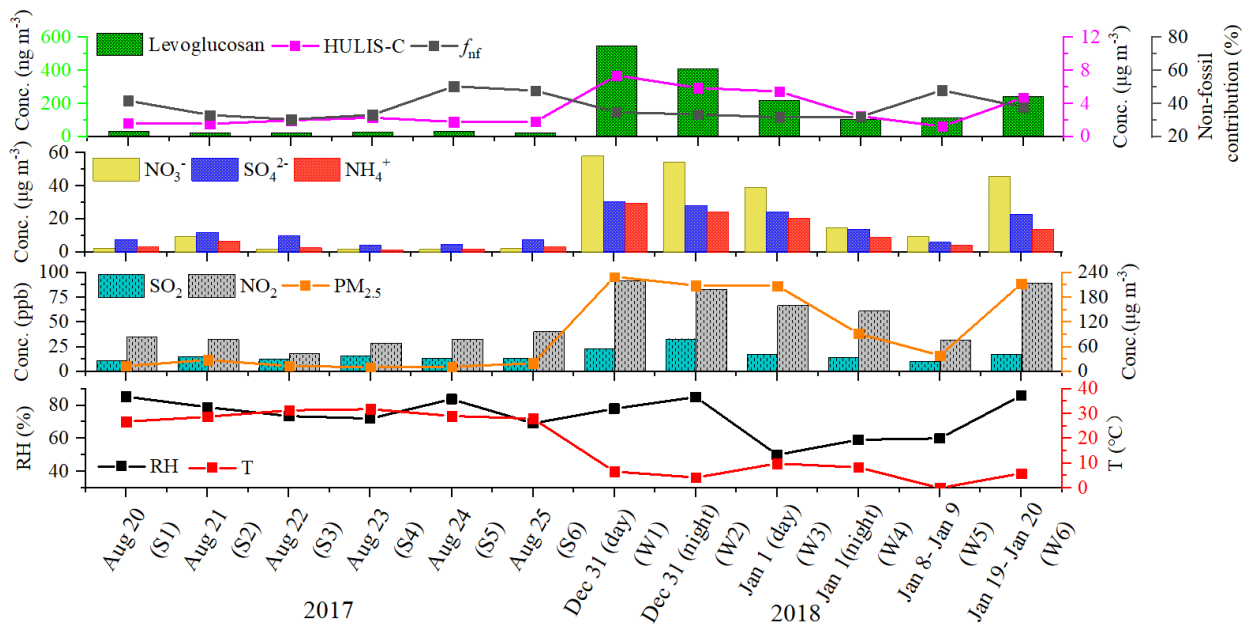
972 Zhang, Y., Forrister, H., Liu, J., Dibb, J., Anderson, B., Schwarz, J. P., Perring, A. E., Jimenez, J.
973 L., Campuzano-Jost, P., Wang, Y., Nenes, A., and Weber, R. J.: Top-of-atmosphere radiative
974 forcing affected by brown carbon in the upper troposphere, *Nat. Geosci.*, 10, 486-489,
975 10.1038/NGEO2960, 2017.

976 Zhao, M., Qiao, T., Li, Y., Tang, X., Xiu, G., and Yu, J. Z.: Temporal variations and source
977 apportionment of Hulis-C in PM_{2.5} in urban Shanghai, *Sci. Total. Environ.*, 571, 18-26,
978 10.1016/j.scitotenv.2016.07.127, 2016.

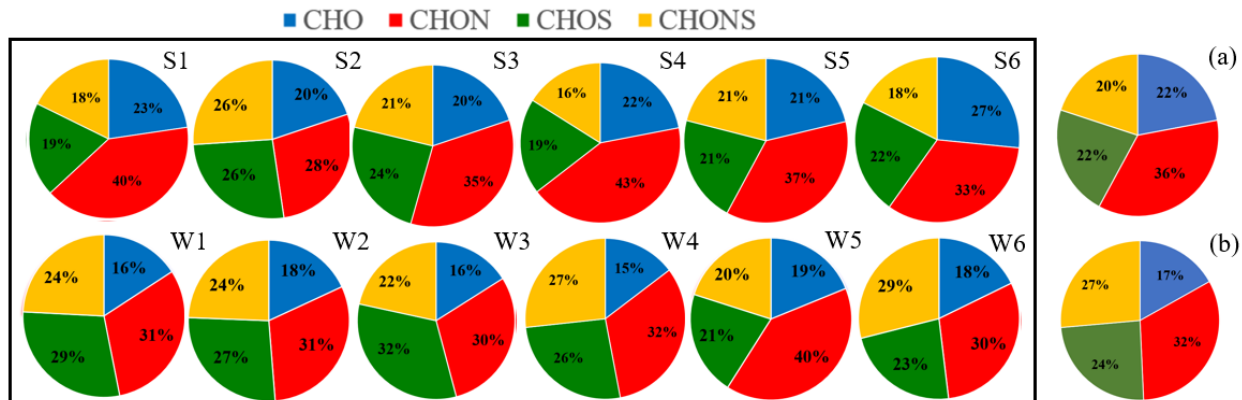
979 Zhao, Y., Hallar, A. G., and Mazzoleni, L. R.: Atmospheric organic matter in clouds: exact masses
980 and molecular formula identification using ultrahigh-resolution FT-ICR mass spectrometry,
981 *Atmos. Chem. Phys.*, 13, 12343-12362, 10.5194/acp-13-12343-2013, 2013.

982 Zheng, G., He, K., Duan, F., Cheng, Y., and Ma, Y.: Measurement of humic-like substances in
983 aerosols: A review, *Environ. Pollut.*, 181, 301-314, 10.1016/j.envpol.2013.05.055, 2013.

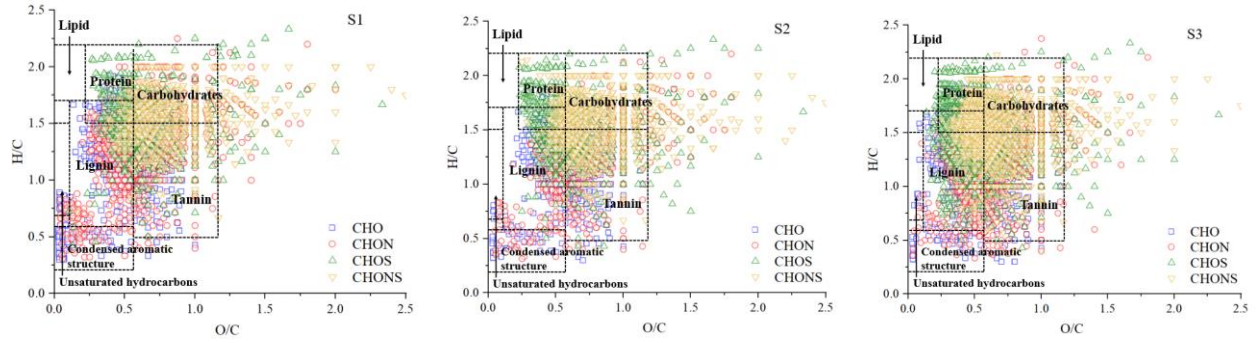
984 Zheng, Y., Chen, Q., Cheng, X., Mohr, C., Cai, J., Huang, W., Shrivastava, M., Ye, P., Fu, P., Shi,
985 X., Ge, Y., Liao, K., Miao, R., Qiu, X., Koenig, T. K., and Chen, S.: Precursors and pathways
986 leading to enhanced secondary organic aerosol formation during severe haze episodes, *Environ.*
987 *Sci. Technol.*, 10.1021/acs.est.1c04255, 2021.



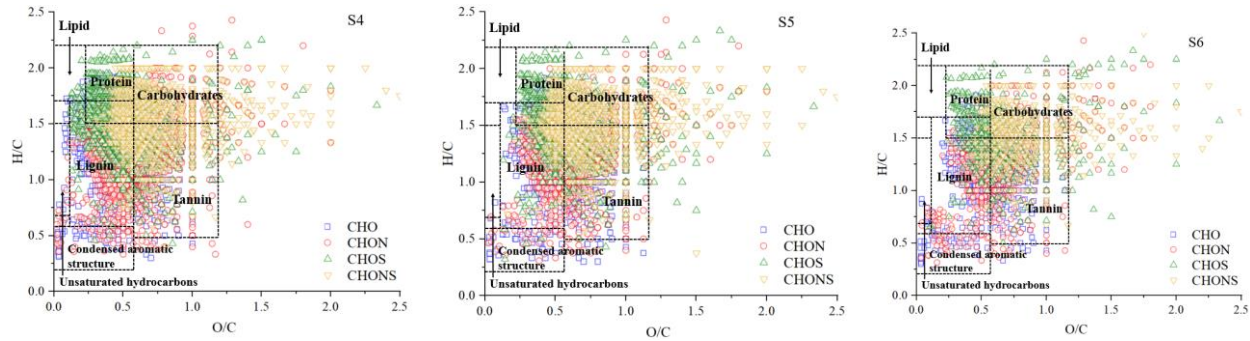
988
 989 Figure 1. Time series of non-fossil contributions to HULIS-C, the mass concentrations of HULIS-
 990 C, Levoglucosan, NO_3^- , SO_4^{2-} , NH_4^+ , SO_2 , NO_2 , and $\text{PM}_{2.5}$, relative humidity, and temperature
 991 during the study periods.



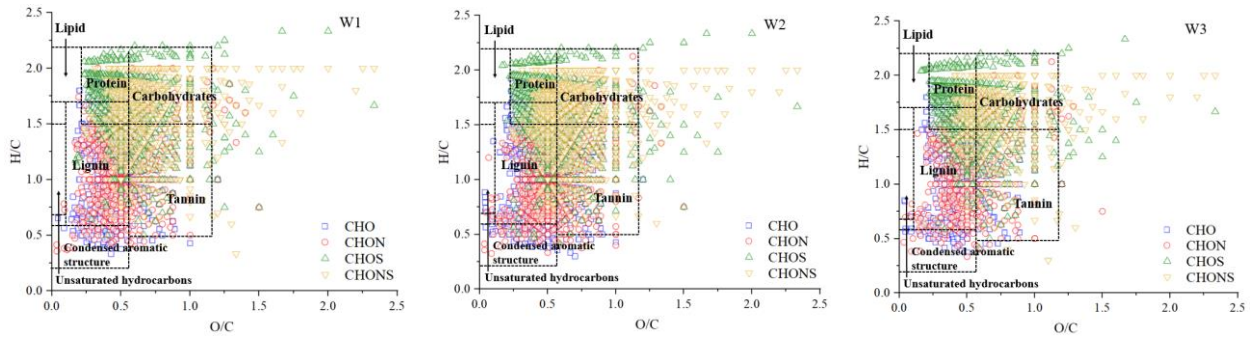
992
 993 Figure 2. Pie graph of the number percentages of each elemental formula group for the 12 samples
 994 plotted in the box and the averaged number percentages of each elemental formula group for the
 995 summer samples (a) and winter samples (b).



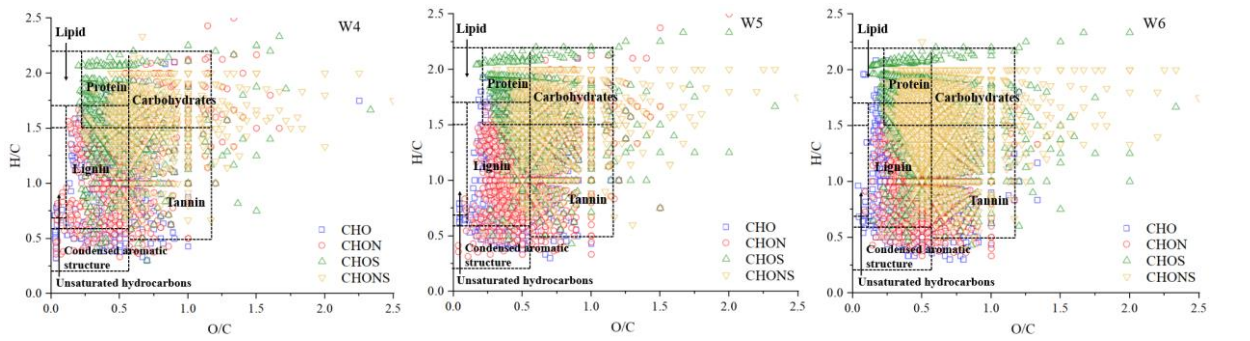
996



997



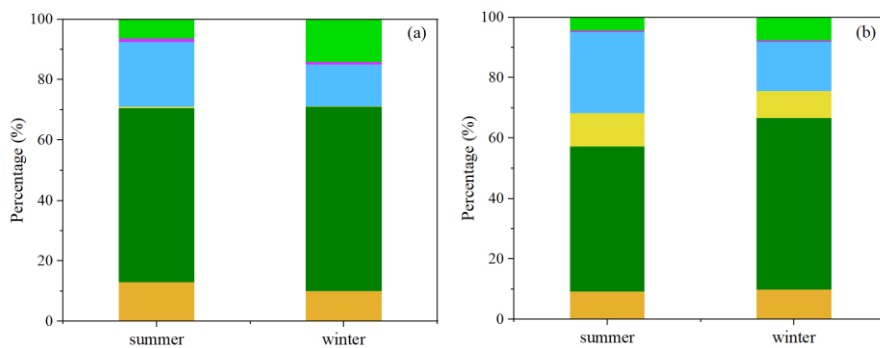
998



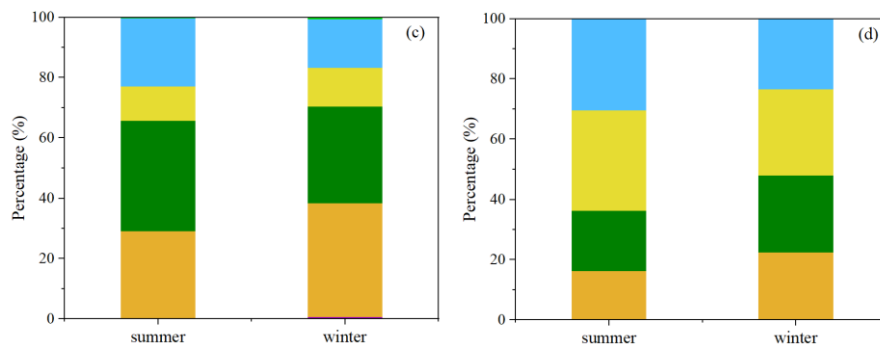
999

1000 Figure 3. Van Krevelen diagrams of the 12 samples.

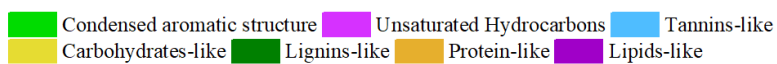
1001



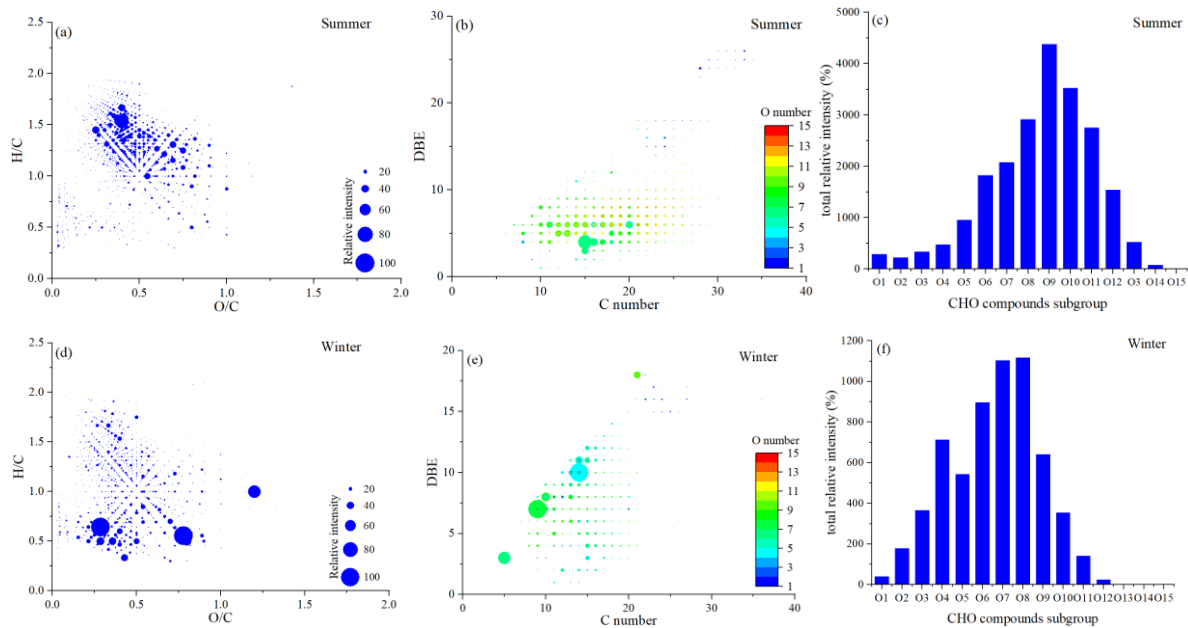
1002



1003



1004 Figure 4. Contributions of seven categories in CHO (a), CHON (b), CHOS (c), and CHONS (d)
1005 compounds.

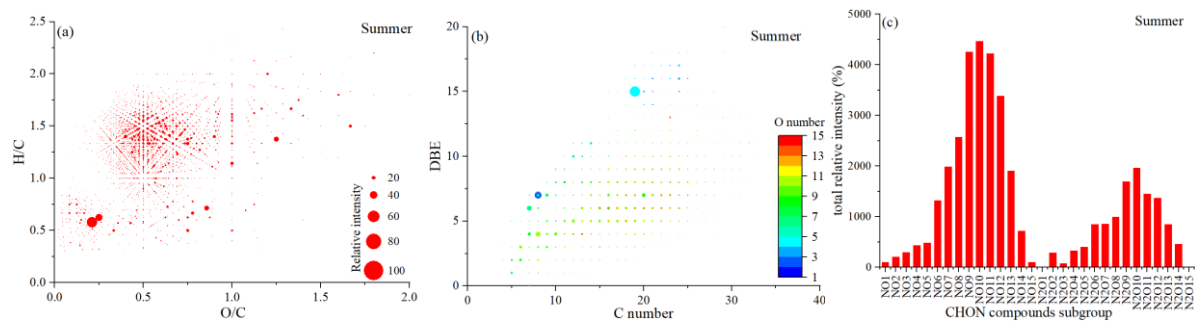


1006

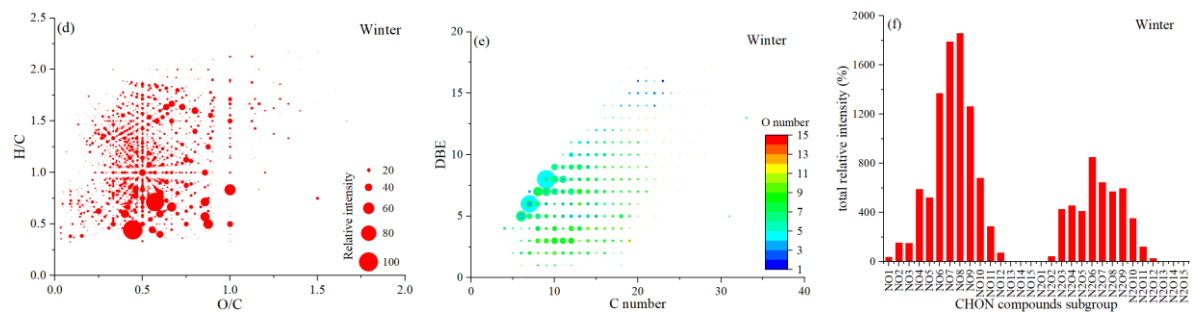
1007

1008 Figure 5. Van Krevelen diagram ((a) and (d)), plot of DBE values vs carbon atom numbers ((b)
 1009 and (e)), and the total relative intensity of each subgroup ((c) and (f)) for the CHO compounds in
 1010 summer and winter.

1011

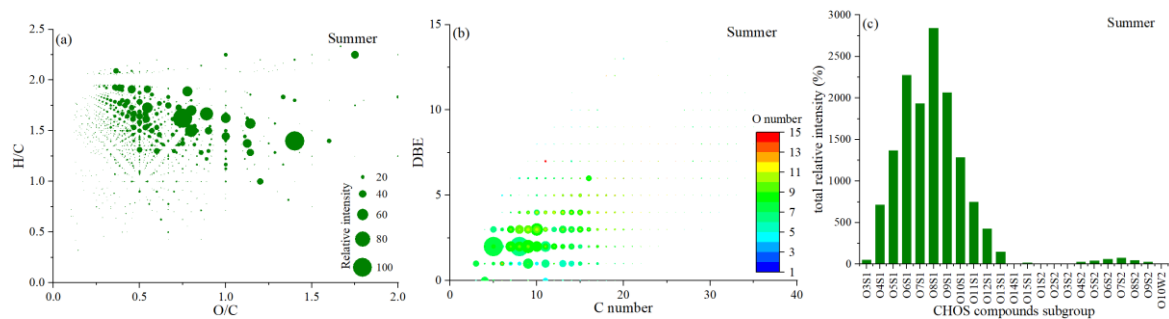


1012

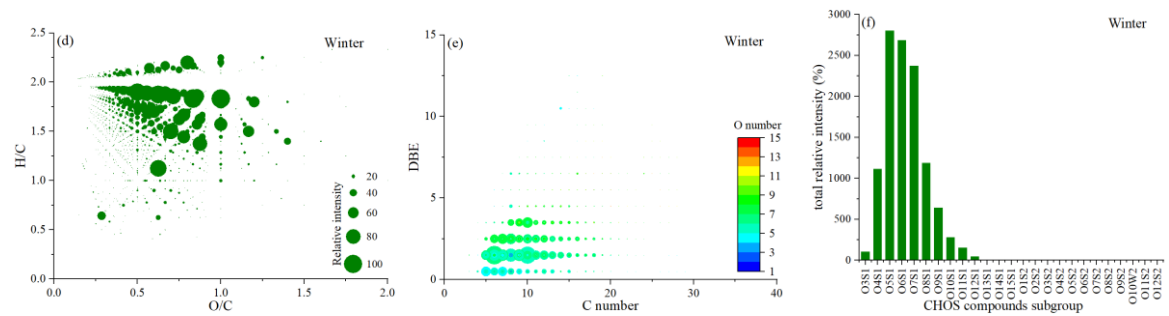


1013 Figure 6. Van Krevelen diagram ((a) and (d)), plot of DBE values vs carbon atom numbers ((b)
1014 and (e)), and the total relative intensity of each subgroup ((c) and (f)) for the CHON compounds
1015 in summer and winter.

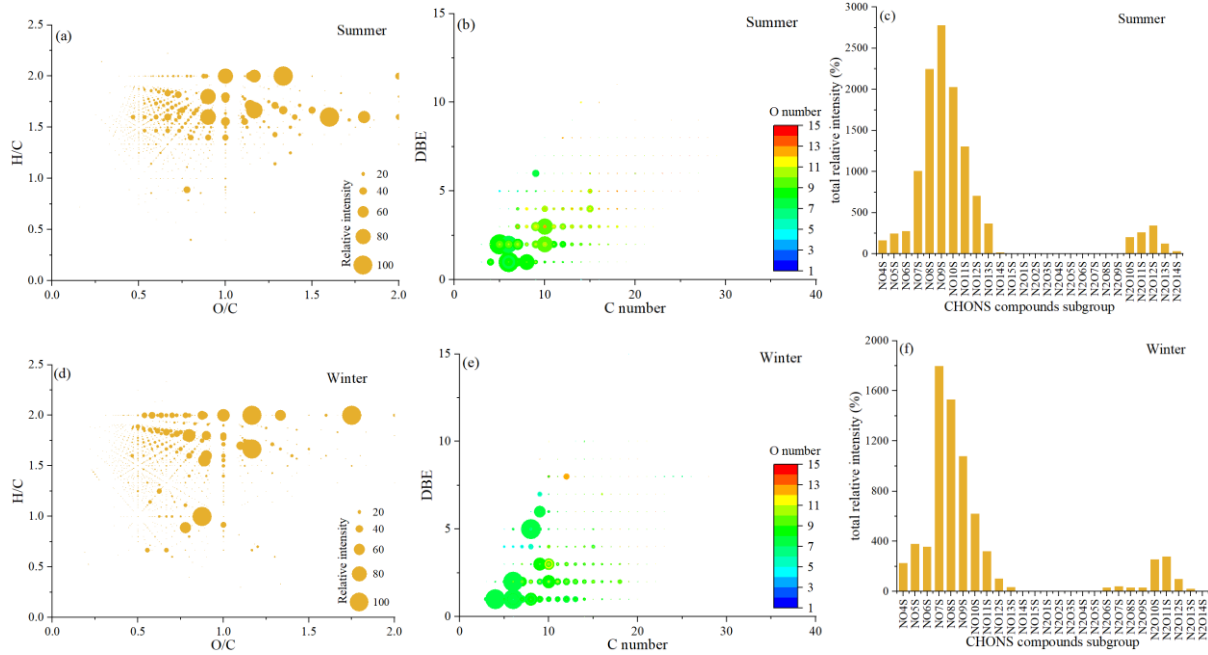
1016



1017



1018 Figure 7. Van Krevelen diagram ((a) and (d)), plot of DBE values vs carbon atom numbers ((b)
1019 and (e)), and the total relative intensity of each subgroup ((c) and (f)) for the CHOS compounds in
1020 summer and winter.

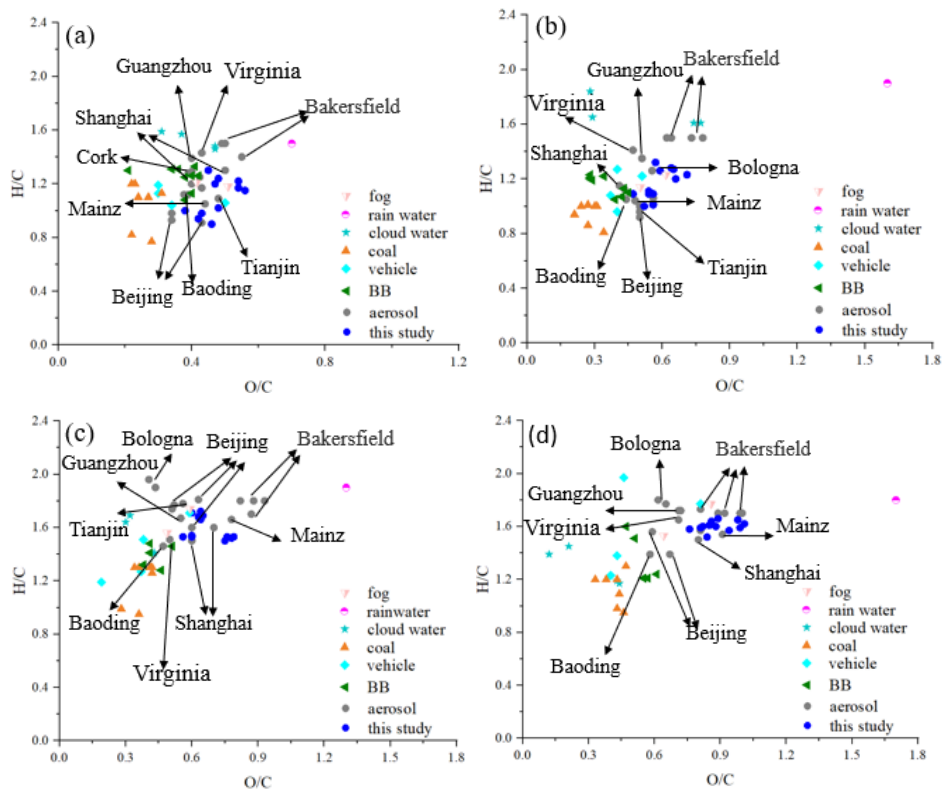


1021

1022

1023 Figure 8. Van Krevelen diagram ((a) and (d)), plot of DBE values vs carbon atom numbers ((b)
 1024 and (e)), and the total relative intensity of each subgroup ((c) and (f)) for the CHONS compounds
 1025 in summer and winter.

1026



1027

1028

1029 Figure 9. Comparison of O/C and H/C ratios of water soluble organic compounds in different
 1030 atmospheric media in CHO (a), CHON (b), CHOS (c), and CHONS (d) compounds.